

SAND79-8202  
Unlimited Release

## Hydrogen Compatibility of Structural Materials for Energy Storage and Transmission

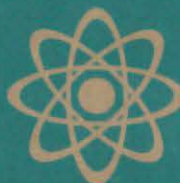
W. R. Hoover, J. J. Iannucci, S. L. Robinson, J. R. Spingarn, R. E. Stoltz

Prepared by Sandia Laboratories, Albuquerque, New Mexico 87115  
and Livermore, California 94550 for the United States Department  
of Energy under Contract DE-AC04-76DP00789.

Printed February 1980



Sandia Laboratories  
energy report



Issued by Sandia Laboratories, operated for the United States Department of Energy by Sandia Corporation.

---

---

#### NOTICE

This report was prepared as an account of work sponsored by the United States Government. Neither the United States nor the United States Department of Energy, nor any of their employees, nor any of their contractors, subcontractors, or their employees, makes any warranty, express or implied, or assumes any legal liability or responsibility for the accuracy, completeness or usefulness of any information, apparatus, product or process disclosed, or represents that its use would not infringe privately owned rights.

Printed in the United States of America  
Available from  
National Technical Information Service  
U. S. Department of Commerce  
5285 Port Royal Road  
Springfield, VA 22161  
Price: Printed Copy \$5.25 ; Microfiche \$3.00

SAND79-8202  
Unlimited Release  
Printed February 1980

HYDROGEN COMPATIBILITY OF STRUCTURAL MATERIALS  
FOR ENERGY STORAGE AND TRANSMISSION

W. R. Hoover  
Materials Development Division 8312

J. J. Iannucci  
Energy Systems Studies Division 8326

S. L. Robinson  
J. R. Spingarn  
R. E. Stoltz  
Materials Development Division 8312  
Sandia Laboratories, Livermore

Annual Report for the Period 10/1/78-9/30/79

Abstract

This annual report documents the activities and contributions accomplished during FY79 on a research contract aimed at assessing the feasibility of transporting hydrogen gas through the existing natural gas pipeline network. Studies of the hydrogen-induced degradation of pipeline steels reveal that hydrogen can be transported in these steels if a number of precautions are taken. These issues are discussed and plans for further research are presented.

## Table of Contents

	<u>Page</u>
I. Summary, W. R. Hoover	5
II. Burst Testing, S. L. Robinson	7
III. Experimental Pipeline Operation, S. L. Robinson	15
IV. Fracture Toughness Measurements of Ferritic Steels in High Pressure Hydrogen, R. E. Stoltz	22
V. Hydrogen Embrittlement of Pipeline Weldments, J. R. Spingarn	37
VI. Economics of Hydrogen Storage J. J. Iannucci and S. L. Robinson	53

Hydrogen Compatibility of Structural Materials for Energy Storage  
and Transmission

I. Summary

W. R. Hoover

This research program is focused on establishing the feasibility of transporting hydrogen gas through the natural gas pipeline network. As such, the primary emphasis has been to assess the hydrogen-induced degradation of pipeline steels. This study has included both the operation of an experimental hydrogen pipeline and extensive laboratory testing of typical pipeline steels and their weldments in gaseous hydrogen.

The results to date indicate that gaseous hydrogen can be transported through the natural gas pipeline network if (a) working pressures are reduced in order to maintain current safety margins and (b) hydrogen accelerated fatigue crack growth can be characterized and controlled. Our studies have shown that hydrogen-induced slow crack growth is not a significant concern. In addition, we have established that typical pipeline weldments are no more susceptible to hydrogen embrittlement than are the parent metals.

In addition to the normal activities conducted under this contract, we report here the results of a study of hydrogen storage economics. The results are reported here for completeness even though these activities were a special task.

The technical achievements of FY79 which are discussed in detail in the following sections are highlighted by the following major conclusions:

1. Hydrogen induced slow crack growth does not appear to be a major concern in typical pipeline steels. Gaseous hydrogen does, however, degrade the burst strengths of flawed pipeline segments and significantly accelerates fatigue crack growth rates.
2. Techniques have been developed to measure the fracture toughness,  $J_{IC}$ , of pipeline steels in high pressure hydrogen. Preliminary results indicate that the  $J_{IC}$  of these steels is reduced by ~ 60% in 1000 psig hydrogen.

3. Tensile tests of both laboratory simulations of pipeline weldments and actual pipeline weldments indicate that neither the fusion zone nor the heat affected zone are more susceptible to hydrogen embrittlement than the parent metals.
4. Two rather extensive systems studies considering the fixed-site storage of hydrogen gas have been completed. For large scale storage, it was concluded that underground storage is the most economical option and is available in sufficient quantity. For smaller scale storage, the optimal storage technique is a function of the quantity stored, the cycle rate, and the cost of electrical power.

We anticipate that FY80 will conclude the work on this contract. We expect to complete the data collection on each of the tasks and will attempt to integrate the results into a final report which summarizes the significant findings of this extended research effort.

## II. Burst Testing

S. L. Robinson

### Introduction

Burst testing of pipes is a direct method of assessing their ability to withstand pressure. If an aggressive medium such as hydrogen is to be contained, a direct measure of the prompt or immediate loss of load carrying ability which the pipe experiences may be obtained as a loss in maximum hoop stress at burst. The actual interpretation of the results may be quite complex and is discussed below. Also, the overall pipeline performance using BTU throughput per unit time as a figure of merit is discussed in light of the burst test results.

### Purposes

This burst testing program has two objectives. The first objective is to provide "factor of safety" information which will indicate hydrogen pressure limits under dynamic or rapid test conditions. The second objective is to develop metallurgical and mechanical understanding of embrittlement phenomena.

### Test Method

The test procedure was to pressurize flawed pipes to failure using the sequence: 0 to 1000 psi hydrogen, followed by nitrogen gas to burst. In this manner the "hydrogen embrittlement potential," which depends upon hydrogen pressure, is kept constant. Baseline tests using only nitrogen gas were also performed. Both internal and external pipe flaws have been tested. Lathe-cut and EDM (Electro-Discharge Machining) flaws have been tested in the internally flawed configuration. Careful measurement of geometry and burst pressure, and examination of fracture surfaces was performed. The pressurization rate was 100 psi/min in the tests. Actual burst testing was performed at an ambient temperature of  $50 \pm 5^\circ\text{F}$ .

### Burst Test Data

In the previous report (SAND79-8200) the burst test data was presented, for internal longitudinal lathe cut flaws in A106-B steel pipe. An expanded test matrix with hydrogen pressure, flaw depth and greater range of lengths

as variables, was designed using the principals of factorial experimental design (the particular form chosen is a 3-level Box-Benken design). The test matrix is shown in Figure 1A, for internal EDM-cut flaws. However, the experiment was damaged by contamination of the hydrogen gas with oxygen in amounts to 0.9%, sufficient to destroy all traces of hydrogen embrittlement (Hoffman and Rauls, 1962).<sup>(1)</sup> (This problem had not been encountered previously in the burst testing facility. Rebuilding the pumps has solved the contamination problem.) Consequently the test results are indicative of inert gas testing only. The data is summarized in Figure 1B. The data and statistics developed will be useful as a baseline when the tests are completed (burst test specimens have been reordered). Data from both burst test series have been plotted in Figure 2, for comparison. The strength properties of the two heats of material, listed in Table I are noticeably different; the behavior differences are attributed to these strength differences.

### Analysis

The apparent fracture toughness of the flawed pipes may be calculated from the burst test data. Using the Irwin half-penny crack analysis<sup>†</sup>, the stress intensity of fracture is calculated from

$$K = \left[ \frac{\pi a}{Q} \right]^{1/2} \sigma_H^* \quad (1)$$

In (1), "a" is the crack half-length, Q is a shape factor, and  $\sigma_H^*$  the nominal stress at fracture is given by

$$\sigma_H^* = \sigma_H \frac{k_S}{k_P} \quad (2)$$

where  $\sigma_H$  is the pressure hoop stress, and  $k_S/k_P$  is the ratio of the shell stress intensity to the flat plate stress intensity for the given flaw. The ratio  $k_S/k_P$  is calculated by Erdogan and Ratwani (2) for through-cracks. Battelle Laboratories used through-crack stress intensification factors to successfully correlate part through-crack failures (3), justifying this approach.

---

<sup>†</sup>The analysis used is the generalized flat elliptical crack in an infinite solid with the crack plane normal to the stress, due to A. Green and I. Sneddon, Proc. Cambridge Phil Soc. Vol 46, p. 159-163, 1950. The initial calculations are due to Irwin and the generalized analysis will be referred to by that name. The analysis applies to a linear elastic material and for penetrations less than 50%. Additional correction factors are available for 1) the effect of a free surface, 2) local plastic deformation and 3) the effects of a pressurized crack face. These corrections will be incorporated shortly.

The results of the calculation are summarized in Table II. A 25% reduction in toughness in 1000 psig hydrogen in thin wall pipe will cause the 15% loss in burst pressure reported previously (SAND79-8200). This result may be compared to the calculation in our previous report in which a 15% loss in toughness was obtained, using an empirical methodology. The magnitude of this loss is similar to that reported by Stoltz (this report) in A516 grade 70 steel in spite of the differences in crack orientation and test procedure.

The predicted loss of toughness has several implications for hydrogen pipeline operation and BTU throughput capability. First, the factor of safety as measured in either (a) a conventional burst test or by (b) fracture toughness methods, is reduced by the presence of hydrogen. To attain an equivalent factor of safety in the burst test rating of 1000 psi H<sub>2</sub>, the pressure must be reduced to 85% of the inert gas rating.\* The fracture toughness rating is based on an assumed final inspection by hydrotest at 150% Maximum Allowed Working Pressure (MAWP). This assures that any surviving flaw has a stress intensity of less than  $\frac{2}{3} K_{inert}^{critical}$ . However, 1000 psi H<sub>2</sub> reduces the toughness to  $K_{H_2}^{critical} \sim \frac{3}{4} K_{inert}^{critical}$ . Therefore, at 100% MAWP the possible limiting flaw would be stressed to  $\frac{\frac{2}{3} K_{inert}^{critical}}{\frac{3}{4} K_{inert}^{critical}} = 90\% K_{inert}^{critical}$ . To give the same factor of safety on stress intensities as for methane operation (factor of safety =  $K_{critical}/K_{operational}$ ) without re-hydrotesting, the MAWP must be reduced to  $\frac{2}{3} K_{H_2}^C = (\frac{2}{3})(\frac{3}{4})K_{inert}^C = \frac{1}{2} K_{inert}^C$ . The new operating pressure is then  $\frac{1/2}{2/3} (MAWP)_{inert} = 75\% (MAWP)_{inert} = (MAWP)_{H_2}$ . This is a more severe pressure reduction than the burst test results imply. Therefore, depending on the methodology used, the working pressures of a pipeline must be reduced from 15% to 25% if hydrogen is to be transported.

The BTU throughputs of hydrogen compared to methane can now be calculated. According to Gregory (5) equivalent BTU throughput requires 120% of the pressure used to transmit methane, owing to competing factors of viscosity (low for H<sub>2</sub>) and compressibility (worse for H<sub>2</sub>). BTU throughput is approximately linear with pressure, thus in the burst-test rated case,  $\dot{Q}_{H_2} = \frac{.85 P_{methane}}{1.20 P_{methane}} = 0.71 \dot{Q}_{methane}$ . In the toughness controlled case,  $\dot{Q}_{H_2} = \frac{.75 P_{methane}}{1.20 P_{methane}} = 0.63 \dot{Q}_{methane}$ . If lowered factors of safety can be accepted, or if re-hydrotesting to higher pressures can be performed then these calculated throughputs may be raised.

\*Assuming methane to be inert, as indicated by Nelson (4).

TABLE I  
STRENGTH PROPERTIES AND MATERIAL ANALYSES

Analysis	C	Mn	Si	P	S	$\sigma_y$ (ksi)	$\sigma_{uts}$ (ksi)	%EL
A	.15	.41	.30	.015	.015	57.89	70.1	40
B	.26	.79	.17	.013	.033	45.9	77.0	35

TABLE II  
FIRST ORDER TOUGHNESS DATA CALCULATED FROM BURST TEST DATA

Materials	$K_Q^* \text{KSI}\sqrt{\text{IN}}$ (Air)	$K_Q^* \text{KSI}\sqrt{\text{IN}}$ (1000 psi Hydrogen)	Section <sup>†</sup> Thickness
A	104	77	.090 inches
B	93	(incomplete)	.120 inches

<sup>†</sup>Section thickness effects may be present, which would account in part for the differences seen in Figure 2.

\*See footnote, page 8.

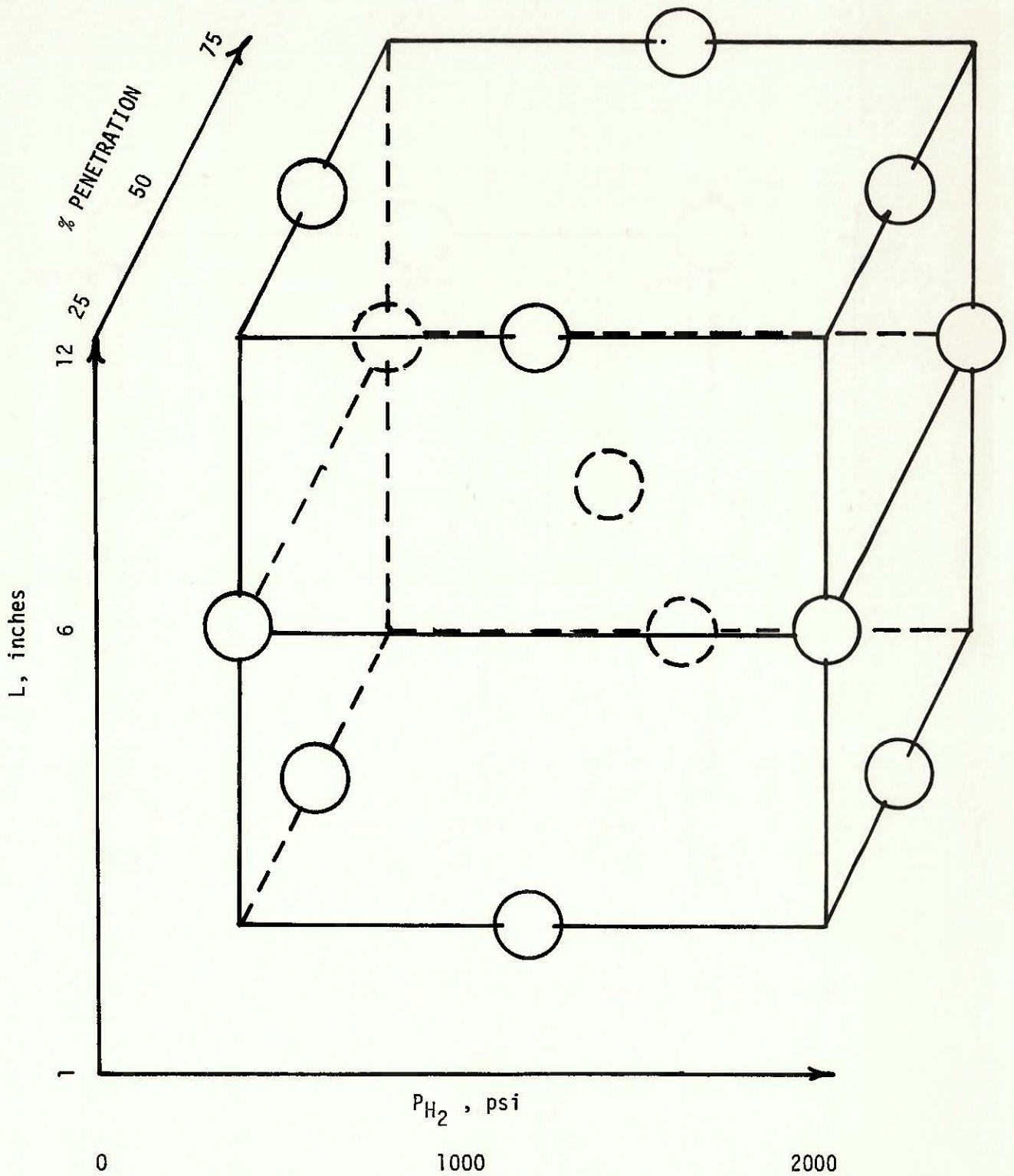


Figure 1A. Three-level Box-Benken Experimental Design Applied to Burst Testing of Flawed Pipes.

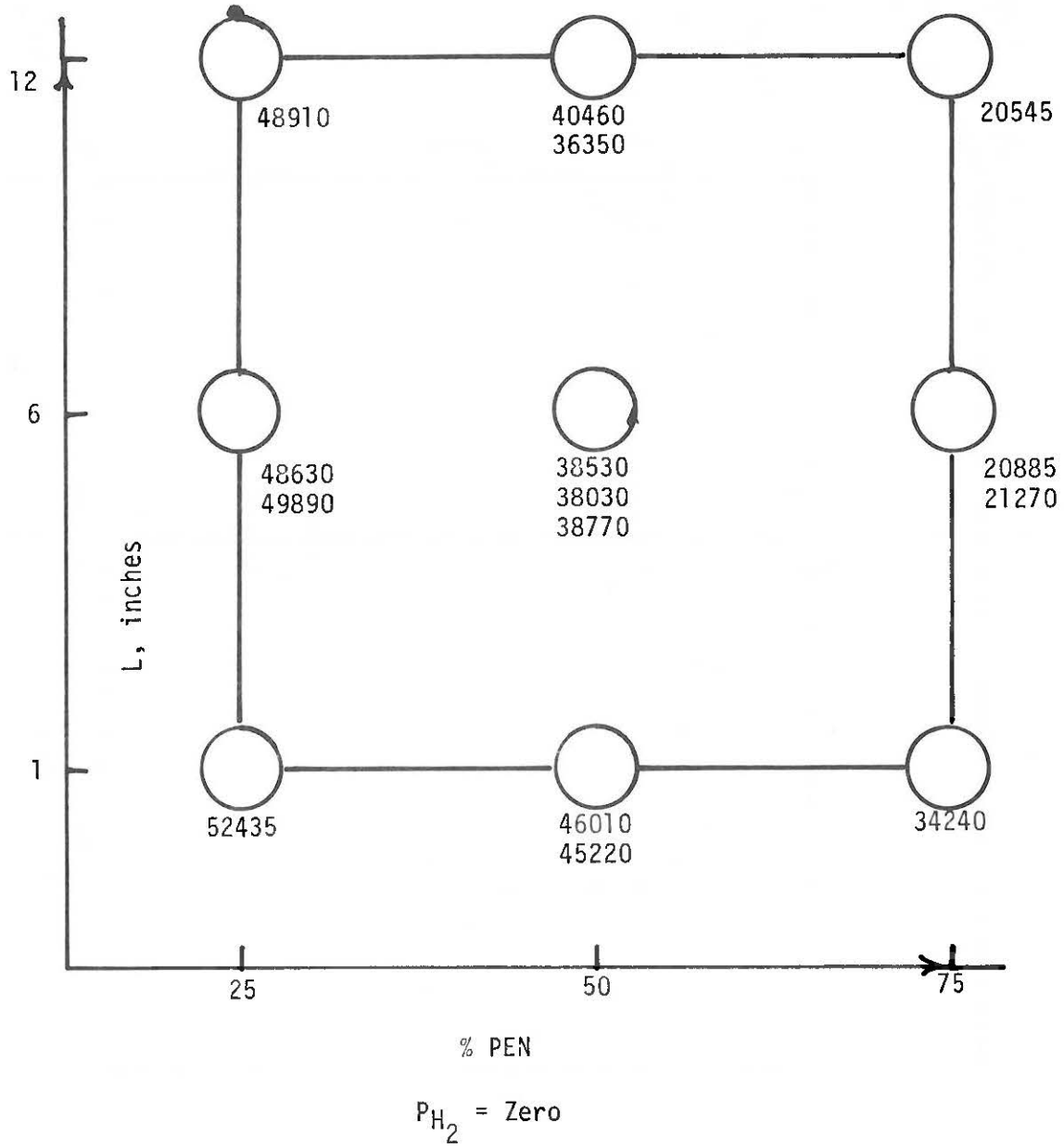


Figure 1B. Nominal Fracture Strengths of Burst Test Pipes with Oxygen Contamination.

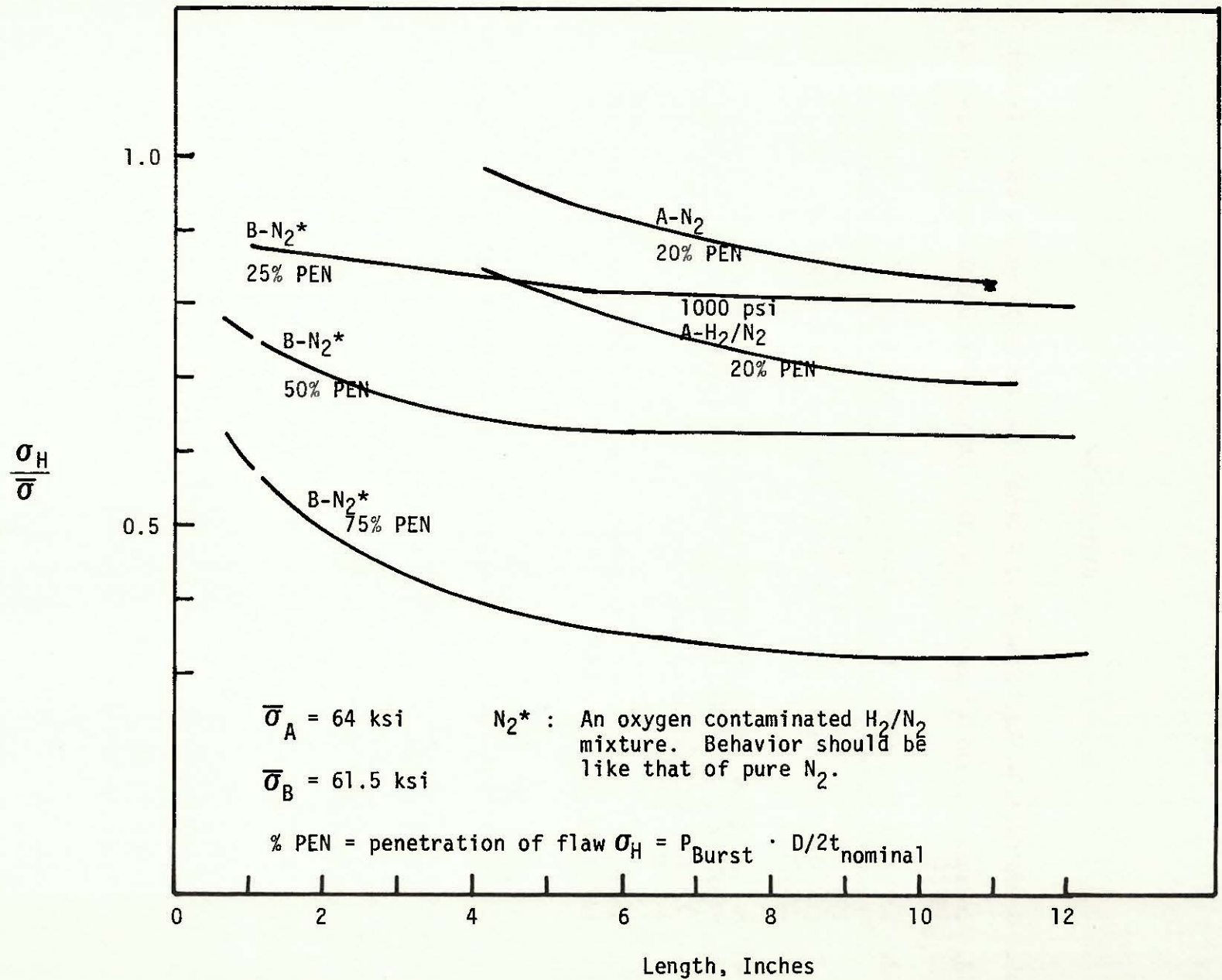


Figure 2. Normalized Burst Test Data for Internally Flawed A-106 Grade B Steel Pipes Nominally of 4 Inch Diameter.

## BIBLIOGRAPHY

1. W. Hoffman, W. Rauls, *Welding Journal*, 44, Research Suppl. 225-5 (1965).
2. Erdogan, F. and Ratwani, M., *Nuclear Engineering and Design*, 20 (265-286) 1972.
3. Duffy, A. R., Eiber, R. J. Maxey, W. A. Recent Work on Flaw Behavior In Pressure Vessels, in *Practical Fracture Mechanics for Structural Steel*, 1969, United Kingdom Atomic Energy Authority; see also 5th Symposium on Line Pipe Research, November 1974, American Gas Association, Cat. No. L30174.
4. H. E. Nelson, Hydrogen Induced Slow Crack Growth of a Plain Carbon Pipeline Steel Under Conditions of Cyclic Loading, p. 602 in Effect of Hydrogen on Behavior of Metals, Eds. A. W. Thompson, I. M. Bernstein, A.I.M.E., 1976.
5. Gregory, D. P., A Hydrogen-Energy System, The American Gas Association, 1973, Catalog No. L21173.

### III. Experimental Pipeline Operation

S. L. Robinson

#### Introduction

Prompt losses in the ability of a pipe to safely carry high pressure hydrogen were assessed by the burst test. However, long exposure times are required to assess long term losses in properties because short time test methods are not yet adequate to predict long-term performance. To answer this need, the experimental hydrogen pipeline loop was constructed to expose pressurized pipe specimens to hydrogen for extended periods of time.

#### Purpose

Pipeline testing is intended to gather data on the effects of long-term exposure of flawed and unflawed pipes to high pressure hydrogen in a pipeline environment. The identification of sustained load cracking is the principal concern.

#### Testing Status

Test Cycle III is in progress, having begun 1 July 1979. Tests in progress are listed in Table I, which includes the time of exposure of each test assembly. A hydrogen pump failure was experienced in late September 1979. The pipeline will continue in static operation until the end of Cycle III in order not to introduce large amplitude fatigue cycles (high  $\Delta K$ , low R ratio) into the test modules in the pipeline.

Shortly after the initiation of Cycle III, transducers placed on the two most severely flawed modules began indicating pressure increases of the order of 10 psi compared to an initial helium pressure of 20 psi. The interpretation of these changes is difficult because of temperature variations in the pipeline. However two analyses were performed. First a permeation calculation of the flawed area was performed. Using limiting case assumptions, hydrogen concentration in the helium due to permeation through the flaw was predicted to be about 0.05 v/o hydrogen. Second, gas samples were drawn from the test assembly annulus and analyzed for hydrogen, giving measured values of 0.76 and 0.67 v/o. These measured values are much higher than the predicted values, yet 10 to 20 fold lower than the transducer values. Transducer error is an attractive explanation, except that only the most severe flaws showed the pressure rise. This conflict has not been resolved. Post-mortem analysis will be required to determine the actual behavior of the flaws in the modules with suspect pressure transducers.

## Analysis of Cycle II Failures

At the beginning of cycle II, two test pipes failed upon pressurization at  $500 \pm 10$  psi after exposure to 1000 psi hydrogen for 6 months, with no evidence of leakage, etc. Analysis of the failures involved stereo scanning electron microscopy of the fracture surface, and stress intensity calculations based on the Irwin method previously discussed under Burst Testing.

Stereo photomicrographs of the fracture surfaces of pipe #34 are shown in Figure 1. The fracture surfaces away from the crack tip were found to have 4 clearly defined fatigue striations prior to the final overload cycle. This corresponds to the number of operationally required pressure cycles, to 0 psig and back to 1000 psig. Table II lists the stress intensity in the 1st, 3rd, and 5th (failure) load application. The measured, and the predicted  $da/dn$  value from laboratory data of Walter and Chandler (1) are in excellent agreement. The conclusion reached is, that hydrogen accelerated low cycle fatigue caused the premature failure of the test pipes. Careful scanning electron microscope study has revealed no evidence suggesting sustained load cracking as the operative crack extension mechanism causing failure.

TABLE I  
TEST CYCLE 3 FLAWS

Assembly Number	Wall Thickness (inches)	Flaw Length (inches)	Flaw Depth (inches)	% Penetration	Location I=internal E=external	Exposure Test (Cycles)
1	0.163	(Butt Weld)	Variable .03-.08	Variable	I	1-3
2	0.103	NONE	-----	-----	-----	1-3
3	0.121	1.0	0.104	86	I	3
4	0.073	10.0	0.015	21	I	1-3
5	0.121	6.0	0.096	79	I	3
6	0.117	3.0	0.093	79	I	2-3
7	0.122	3.0	0.089	73	I	2-3
8	0.126	12.0	0.092	73	I	3
9	0.115	1.0	0.098	85	I	3
10	0.119	3.0	0.100	84	E	3
11	0.117	3.0	0.105	90	I	3
12	0.120	1.0	0.092	77	I	3
13	0.122	10.0	0.088	72	I	2-3
14	0.130	10.0	0.090-	69	I	2-3
15	0.122	12.0	0.090 <sup>+</sup>	74	I	2-3
16	0.123	2.0	0.090	73	I	2-3
17	0.123	6.0	0.099	80	E	3
18	0.118	12.0	0.101	86	E	3
19	0.118	1.0	0.095	81	E	3
20	0.114	1.0	0.098	86	E	3
21	0.119	1.0	0.099	83	I	3

TABLE II

## STRESS INTENSITIES IN LOW CYCLE FATIGUE FAILURE OF TEST PIPE 34

Pressure Cycle Number	Pressure psi	$\Delta K$ KSI $\sqrt{IN}$	(da/dN) Measured	(da/dN) $\dagger$ Predicted	% Penetration
1	0 - 1000	47.0	$2.6 \times 10^{-3}$ inches	1.9-2.0 $\times 10^{-3}$ inches	25
3	0 - 1000	57	$5 \times 10^{-3}$ inches	$4 \times 10^{-3}$ inches (extrapolation)	40
5	0 - 500	50*	---	---	100%

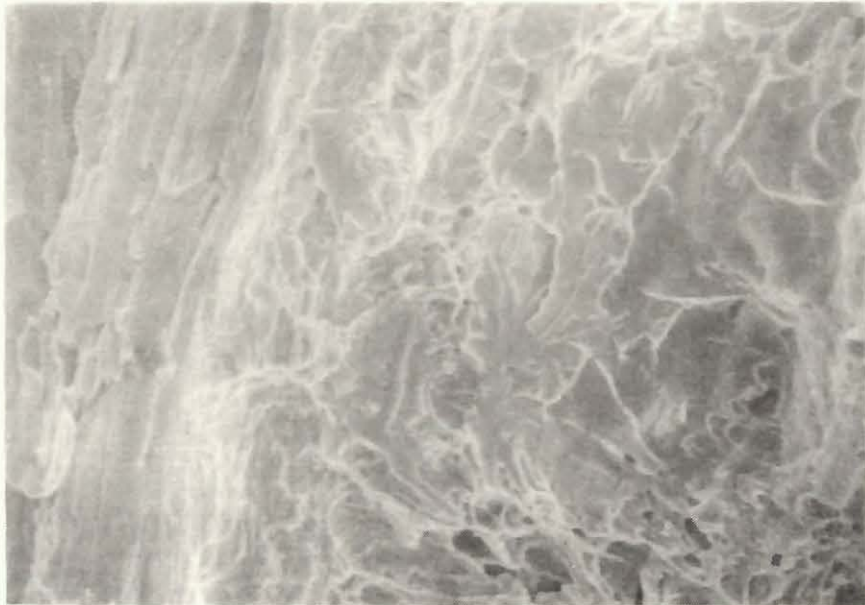
$\dagger$ Data of Walter and Chandler for SA-105 steel at 1000 psi H<sub>2</sub>.

$$K_Q = \pi \frac{a}{Q}^{1/2} \sigma_H \frac{k_s}{k_p}$$

$k_s/k_p = 6.4$  from Erdogan and Ratwani

Crack parameters:  $a = 0.015$  inch, length = 10 inches, 25% penetration,  
initial wall thickness = 0.059 inches.

\*Assumptions of the Irwin analysis break down for PEN > 50%. Corrections are possible but have not been made.



LEFT



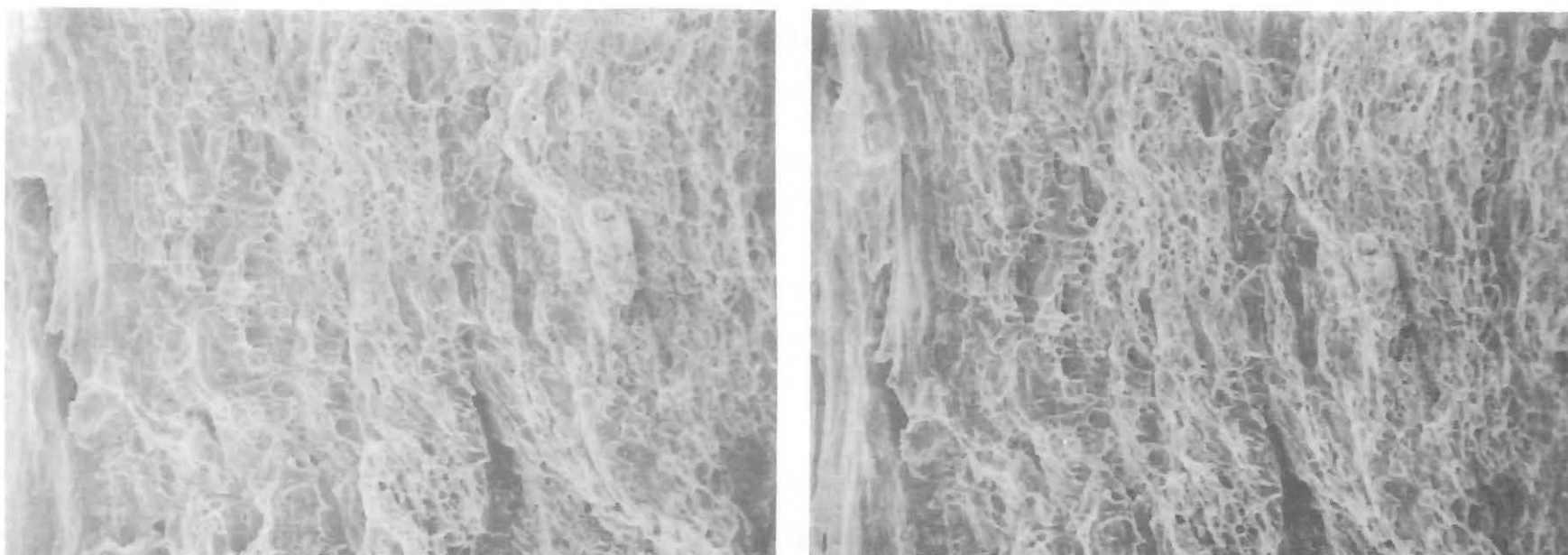
RIGHT

600X

Internal longitudinal 25% v-notch, 10 inches long  
Test pipe #34

FATIGUE FRACTURE NEAR CRACK TIP

Figure 1A. Stereo Scanning Electron Micrographs Near Fatigue Fracture Crack Tip.



LEFT

RIGHT

300X

Test pipe #34

FATIGUE FRACTURE AWAY FROM CRACK TIP

Figure 1B. Stereo Scanning Electron Micrographs Away From Fatigue Fracture Crack Tip.

## BIBLIOGRAPHY

1. Walter, R. J. and Chandler, W. T., Crack Growth in ASME SA-105 Steel in Hydrogen at Ambient Temperature, p. 273 in, Effect of Hydrogen on Behavior of Metals, Eds. A. W. Thompson and I. M. Bernstein, A.I.M.E., 1974.

## IV. Fracture Toughness Measurements of Ferritic Steels in High Pressure Hydrogen

R. E. Stoltz

### Introduction

Measurements of the effect of high pressure hydrogen on the fracture toughness of A516-70 steel have been made in support of our program for evaluating structural materials for hydrogen transport and storage. Efforts in the previous year, FY 1978, concentrated on establishing baseline data in air and the effects of hydrogen at one atmosphere (1). This report deals with the effects of higher hydrogen pressures, 1000-3000 psi, on toughness and fracture resistance.

### Facility Development

Considerable effort was expended in the past year to design and construct an experimental facility for toughness testing in hydrogen at high pressures. The major components of the system include a gas source and purification system, high pressure pump, test vessel, and mechanical loading frame. The goal of the system design is to provide accurate simultaneous recording of the load and specimen displacement for toughness evaluation. Some of the unique features of the system are described below.

The pressure vessel is a 2 inch diameter bore, stainless steel vessel rated to 7500 psi maximum working pressure. This pressure limit allows for manned operation of the facility. Figure 1 is a schematic of the vessel. The pull rod is designed with an integral flange and a balancing pressure chamber so that upon pressurization no resultant load is placed on the sample. This allows for accurate load monitoring external to the vessel. The vessel is also fitted with a four-wire high pressure feed-through so that electrical signals from the internal LVDT displacement gage can be monitored.

A Schaevitz model 099XS-B LVDT and CAS-025 signal conditioner was selected for measuring the strain on the sample itself. The gage is accurate to 0.001 in. out of a 0.100 in. full scale range. Drift tests were conducted to monitor any effects of hydrogen pressure on signal output. No measurable drift was detected at either 1000 or 3000 psi hydrogen pressure over a one hour exposure.

Load vs. load-line-displacement data is recorded in two ways. An analog signal is recorded on a conventional x-y recorder. A digital signal is also recorded on a Nicolet 201 transient data recorder equipped with a floppy disc. The time constant is adjusted to record 200-1000 data points for each load vs. displacement trace. The digital data is then processed by a Textronix

4051 mini-computer. Since the toughness is directly proportional to the area under the load-displacement trace (see below) a program was written to extract this quantity. The x-y plot provided an additional check on the data when necessary.

### Experimental Procedures

All testing was performed on specimens from the A516-70 heat used in the previous study (1). Double edge notch (DEN) samples were used in all tests and are shown in Figure 2. The pressure vessel geometry dictated using an axi-symmetric specimen design. Samples were cut from the starting plate in the L-T orientation, as was done previously. Following the approach of Hickerson (2) only one notch was fatigue precracked, so that hydrogen crack growth occurred only at that location. Tests were performed at 0.02 in/min extension rate in hydrogen gas purified to <1ppm water and oxygen. Following loading, samples were heat tinted and broken open to determine the amount of crack extension. A travelling microscope, accurate to 0.001 in. was used for crack length measurements.

The load-displacement curves were converted to applied J (energy for fracture) by the procedure used by Hickerson (2). The formula for J is given by

$$J = \frac{K}{E} + \frac{1}{Bb} [2(A_T - A_E) - P_e(V_C - V_e)]$$

B and b are the sample thickness (0.250 in) and remaining ligament width, respectively. The elastic crack extension force, K, was determined from the geometry, load and crack length using formulas given in Ref. 3. The remaining values,  $A_T$ ,  $A_E$ ,  $P_e$ ,  $V_C$ ,  $V_e$  are given by Figure 3. The area under the load-displacement curve,  $A_T$ , was that determined from the digitized data. Finally, once J was determined for each sample and condition, the results are plotted on a curve of J vs. crack extension.

### Results

Tabulated results for DEN tests performed in air and at 1000 and 3000 psi hydrogen are given in Table I with the data displayed graphically in Figure 4. A crack blunting line is drawn with slope  $2\sigma_f$  ( $\sigma_f$  is the average of the yield and ultimate strengths or 63,500 psi). The  $J_{IC}$  values are determined at the intersection of the  $J$  vs  $a$  line and the blunting line. These values are given in Table II along with the slope of the  $J$  vs  $a$  curves,  $dJ/da$ .

Fracture surfaces of specimens tested in air and at 1000 and 3000 psi hydrogen were examined by scanning electron microscopy. Figure 5(a) shows the fracture surface generated in air, along with a corresponding typical microstructure taken at the same magnification (Figure 5(b)). Dimple

rupture by void growth and coalescence is the fracture mode in air. The fracture features do not correspond in scale to either the ferrite grain size or pearlite colony size. Rather, as shown at points (A) in the fractograph, small inclusions present in the sample served as void nucleation sites. These inclusions have been identified as alumino-silicate particles and are present due to the use of aluminum as a deoxidizer.

Figures 6 and 7 show the fracture features in 1000 and 3000 psi hydrogen. In all cases a companion photograph showing the microstructure is included so as to compare the size scale of the fracture features with those of the underlying alloy. Void growth is completely suppressed and replaced by a mixed quasi-cleavage and ductile tearing fracture process. Flat regions on the fracture surfaces, Figure 6(c) and 7(c) correspond in size to the free ferrite regions, while the ductile tearing regions correspond to the pearlite colonies. It is not clear whether the inter-lamellar ferrite within the pearlite colonies fails by a cleavage or by a ductile process.

## Discussion

Table II and Figure 4 summarize the results of hydrogen pressure on fracture toughness and stable crack growth resistance. As was the case with 1 atm hydrogen (1) a significant decrease in fracture resistance occurs in hydrogen gas, when compared to air.

In comparing the  $J_{IC}$  values obtained in the current work, approximately 900 in-lb/in<sup>2</sup> in air vs. 250 in-lb/in<sup>2</sup> in 1000-3000 psi hydrogen, with those measured in the earlier study<sup>(1)</sup>, 650 and 350 in-lb/in<sup>2</sup>, some account must be taken for specimen geometry and thickness. The earlier experiments employed a compact geometry with a 0.750 in. thickness, while the present tests used double edge notch samples which were 0.250 in thick. The criteria for a valid test is given by comparing the thickness, B, to the quantity  $25 \frac{J}{\sigma}$ .

For  $b = 0.750$  in, the maximum valid  $J$  would be 1500 in-lb/in<sup>2</sup>. However, for 0.250 this value is only 500 in-lb/in<sup>2</sup>. Thus, the air value for the DEN sample, 900 in-lb/in<sup>2</sup> is most likely an overestimate. The  $J_{IC}$  values in hydrogen, 350 for 1 atm and approximately 250 for 1000-3000 psi gas pressures are all valid and indicate that only a small degradation in toughness occurs at the increased gas pressures. In addition, the slope of the  $J$  vs.  $a$  curves in 1 atm hydrogen and 1000-3000 psi are also in the same range, approximately  $2-3 \times 10^4$  psi. It appears that the effect of hydrogen on toughness and crack resistance undergoes a rapid saturation and that large changes are not evident between 15 psi (1 atm) and 3000 psi hydrogen pressure.

This saturation effect has been observed in other instances of hydrogen assisted fracture. Nelson (4) reports that 18 psi hydrogen accelerates fatigue crack growth rates a factor 100 over that in air. Increasing the pressure to 1000 psi further increases the growth rate only by an additional factor of two. Clark (5) in a review of the effects of hydrogen on sustained load cracking in 4340 shows a saturation in crack growth threshold with hydrogen pressure. The threshold does not change significantly from 100 to 300 psi hydrogen pressure.

The large change in fracture toughness in going from air to low hydrogen pressures (approximately 15 psi) and the saturation in effect at pressures 15-3000 psi suggests that embrittlement is not a simple linear function of lattice solubility. Two possible rate limiting mechanisms exist which may be responsible for the variation in properties with pressure. First, the amount of hydrogen on the surface is related to the surface adsorption kinetics. Experiments in pure iron (6) show that above 1 torr ( $10^{-3}$  atm) the adsorption kinetics are independent of pressure. If the fracture process is related to the adsorption of hydrogen at the crack tip, then significant reductions in fracture resistance should not occur at pressures greater than 1 torr.

Secondly, if dislocation transport of hydrogen is the rate limiting step, the maximum amount of embrittlement will occur once the dislocations are saturated with hydrogen. Tien, et al, (7) calculate that a dislocation core concentration of 1 (one H for each lattice spacing of core) would be present at a room temperature concentration of 3 ppm. This concentration is readily achieved in steels at room temperature. (8) It is presently difficult to distinguish between these two steps in the embrittlement process and experiments at low hydrogen pressures are planned to differentiate between the two effects.

A second observation on hydrogen assisted fracture in low carbon steels like A516 is the lack of sustained load cracking at pressures up to 5000 psi hydrogen (9). The absence of sustained load cracking is most likely related to the quasi-cleavage process, in the following way. In both rising load tests, such as those reported here, and in fatigue tests (4) the ferrite fractures by "quasi-cleavage". The only difference is the presence of fatigue striations in the latter case. However, fatigue striation formation is controlled by plastic deformation. This suggests that plastic deformation is essential to the quasi-cleavage process, so much so that the term cleavage (indicating fracture under normal stresses) may be incorrect. Beacham (10) has shown that in a 1020 steel, hydrogen lowers the yield and flow stress in torsion over a large strain increment. Thus "quasi-cleavage" may be a process of hydrogen assisted flow rather than hydrogen assisted fracture. The key observation necessary to this argument is that the fracture plane in the ferrite is a slip plane not a cleavage plane. Experiments are currently planned to determine the orientation of the fracture plane. A similar situation of transgranular (or cleavage-type) fracture during plastic deformation occurs in tests of pure nickel in hydrogen. It has been shown that hydrogen induces fracture on (111) planes in nickel and that hydrogen lowers the flow stress curve and enhances plastic deformation (11). The fracture process is one of dislocation accumulation on the slip plane and eventual rupture by a slipping-off process. In this case no true cleavage occurs even though a crystallographic fracture plane is observed.

The above discussion has dealt with the similarities of the critical parameters for initiation of fracture and fracture propagation as a function of pressure. Some differences in  $J_{IC}$  and  $d/d_a$  exist between 15 psi and 1000 psi (Table II). Comparing the fracture surface features reveals little differences in the fracture of the free ferrite. Some greater tearing occurs at 15 psi in the pearlite so that differences in toughness and fracture

resistance may be related to the failure of the inter-lamellar ferrite within the pearlite colonies. Since the pearlite acts as a "ductilizing" region, reducing the ferrite volume fraction or spheroidizing the alloys would reduce the toughness in hydrogen. Thus the pearlite microstructure is likely the least sensitive to hydrogen assisted fracture.

### Summary

An experimental facility has been developed for measuring the effect of hydrogen on fracture toughness of pipeline steels. Initial results indicate that hydrogen lowers the critical fracture parameter,  $J_{IC}$ , from 650 in-lb/in<sup>2</sup> in air to ~350 in-lb/in<sup>2</sup> at 15 psi hydrogen and to ~250 in-lb/in<sup>2</sup> at 3000 psi hydrogen. A concomitant reduction in resistance to crack growth, given by the variation in  $\underline{J}$  with crack extension also occurs in hydrogen.

Fractographic analysis shows that hydrogen induces a quasi-cleavage fracture mode in the free ferrite and a tearing across the pearlite. The quasi-cleavage process has a strong component of plastic deformation and is likely caused by hydrogen assisted flow not fracture.

TABLE I  
SUMMARY OF J-TEST DATA

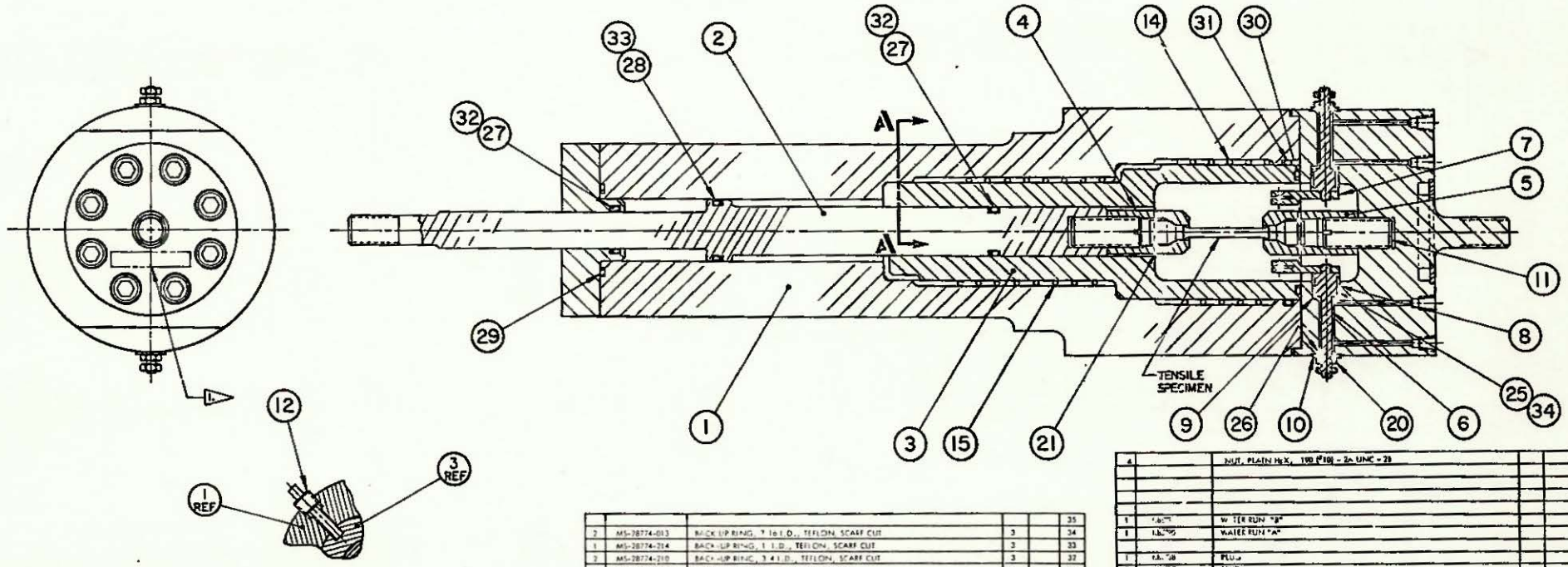
	Sample No.	J, in-lb/in <sup>2</sup>	$\Delta a$ , in
<u>Air</u>	0-3	900	.0075
	0-1A	1200	.0115
	0-4	2500	.0315
<u>1000 psi H<sub>2</sub></u>	1-1	548	.0115
	1-2	828	.0245
	1-3	1298	.0424
	1-4	1560	.0455
<u>3000 psi H<sub>2</sub></u>	3-1	670	.0239
	3-2	806	.0249
	3-3	1294	.0507
	3-4	1804	.1002

TABLE II  
SUMMARY OF J-TEST RESULTS

Environment	J <sub>IC</sub> , in-lb/in <sup>2</sup>	dJ/da, psi
Air	890	6.6 x 10 <sup>4</sup>
1000 psi H <sub>2</sub>	241	2.8 x 10 <sup>4</sup>
1000 psi H <sub>2</sub>	262	2.1 x 10 <sup>4</sup>

MARK DRAWING NUMBER AND ISSUE IN APPROXIMATE LOCATION SHOWN, METHOD OPTIONAL.  
 2. GENERAL REQUIREMENTS AND DRAWING INTERPRETATIONS ARE DEFINED IN 9902000.  
 3. A PRODUCT OF:  
 PARKER SEAL CO.  
 CLEVELAND, OHIO

REV	DATE	DESCRIPTION	APPROVED BY	DATE	ISSUE
A	1-24-75		Spacht		



**SECTION A-A**

QTY	PART NO.	DESCRIPTION	UNIT	ISSUE
2	MS-28774-013	BACK-UP RING, 7 1/2 I.D., TEFLON, SCARF CUT	3	35
1	MS-28774-214	BACK-UP RING, 1 I.D., TEFLON, SCARF CUT	3	33
2	MS-28774-210	BACK-UP RING, 3 4 I.D., TEFLON, SCARF CUT	3	32
1	2-232-V709-90	O-RING, 2-3 4 I.D. X 1 8 W, VITON	3	31
1	2-228-V709-90	O-RING, 2-3 4 I.D. X 1 8 W, VITON	3	30
1	2-225-V709-90	O-RING, 1-5 8 I.D. X 1 8 W, VITON	3	29
1	2-214-V709-90	O-RING, 1 I.D. X 1 8 W, VITON	3	28
2	2-210-V709-90	O-RING, 3 4 I.D. X 1 8 W, VITON	3	27
2	2-106-V709-90	O-RING, 3 16 I.D. X 3 32 W, VITON	3	26
2	2-013-V709-90	O-RING, 7 16 I.D. X 1 16 W, VITON	3	25
				24
				23
				22
2		PIN, SPRING, 1 16 DIA X 7 8 LONG		2

QTY	PART NO.	DESCRIPTION	UNIT	ISSUE
1		BUT. PLAIN H.S., 100 PPI - 2-UNC - 20		20
				19
				18
				17
				16
1	1.67	WATER RUN "B"		15
1	1.67	WATER RUN "A"		14
				13
1	1.67	FLU...		12
2	1.67	STUD		11
2	1.67	WASHER "B"		10
2	1.67	WASHER "A"		9
2	1.67	SP-CER		8
2	1.67	AD-PER, HEATER		7
2	1.67	ELECTRODE		6
1	1.67	GRIP "B"		5
1	1.67	GRIP "A"		4
1	1.67	ROD GUIDE		3
1	1.67	ROD		2
1	1.67	REUSIN...		1

PART OF CONTROL NO. (A) DOCUMENTS (B) AS REQD PER ASSEMBLY (C) PROCESSED MATERIAL (D) AS REQD (E) AS REQD (F) ALTERNATE (G) EXPENSE MATERIAL	DESCRIPTION TENSILE TESTER	NOTE SHEET NO. OF 1
DATE: 1-24-75 APPROVALS: [Signature] ISSUE: A	PART CLASSIFICATION <b>UNCLASSIFIED</b>	TITLE <b>TENSILE TESTER</b>
DWG CLASSIFICATION LEVEL <b>UNCLASSIFIED</b>	SIZE: D CODE IDENT. NO.: 14214 SCALE: 1/1	DWG NUMBER: KBP798 SHEET: 1 OF 1

Figure 1. Schematic of Hydrogen Test Vessel.

K88798

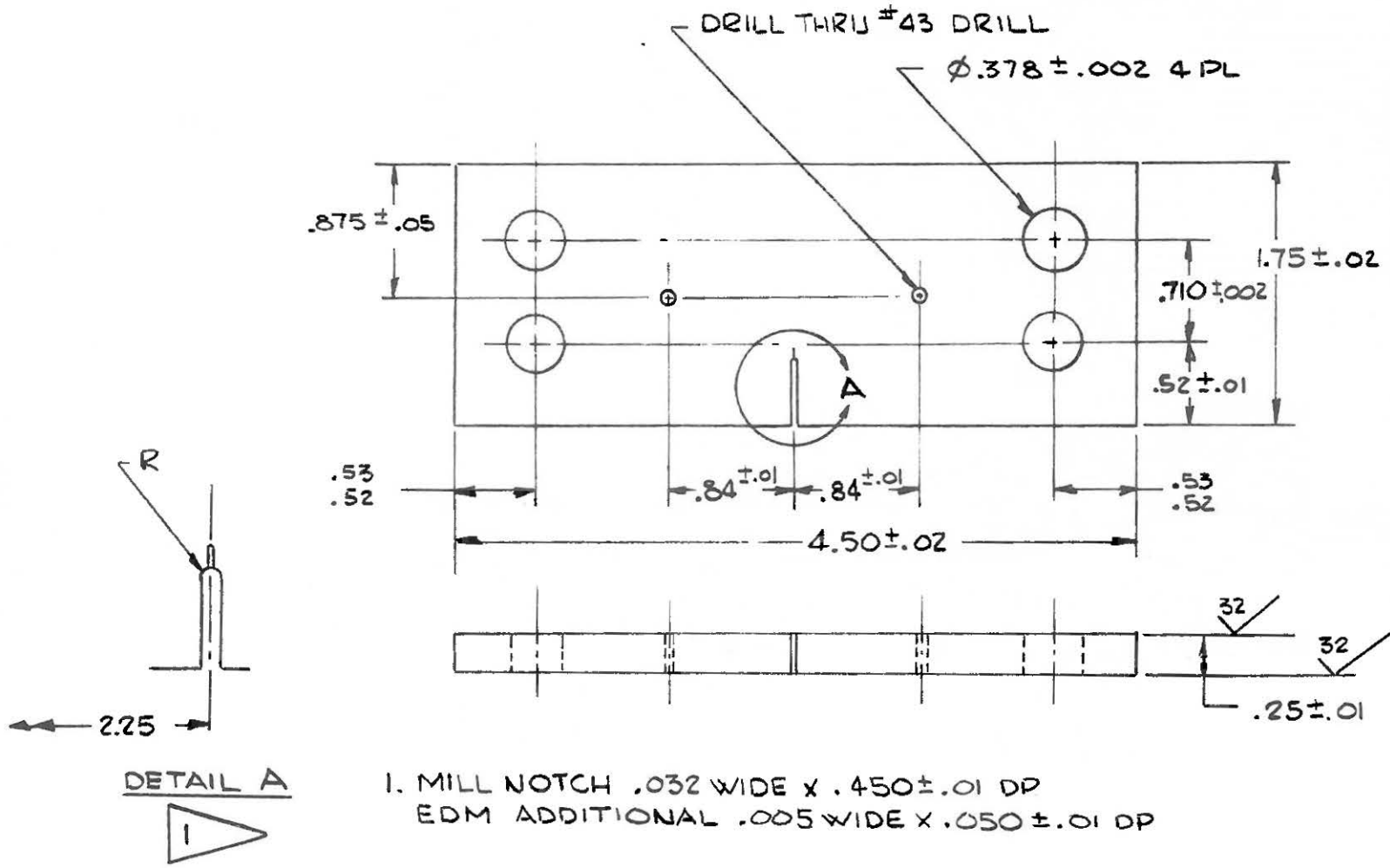
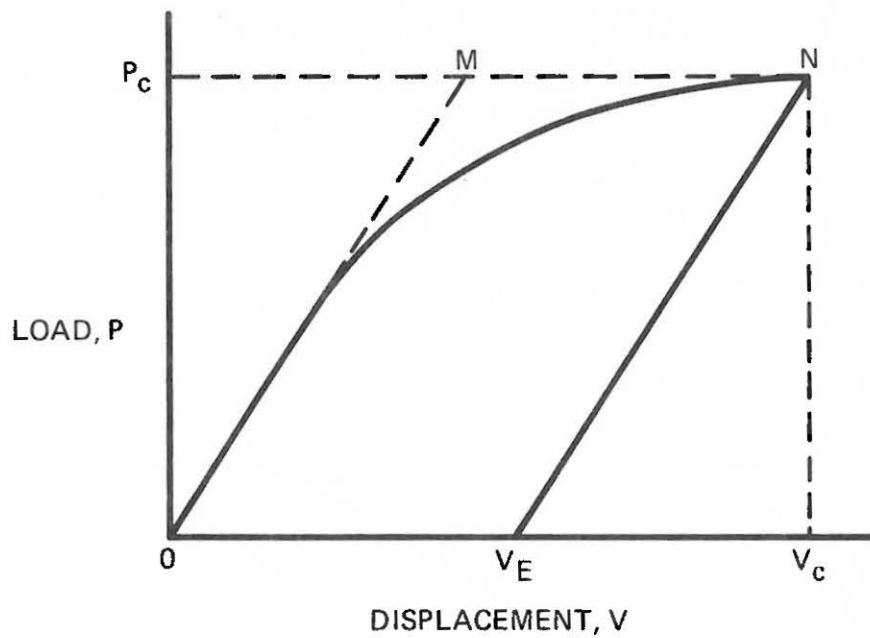


Figure 2. Double Edge Notch Toughness Specimen.



$$A_T = ONV_c = \int_0^{V_c} P dV = \text{AREA UNDER } ONV_c$$

$$A_E = OMV_E = \frac{1}{2} P_c V_E$$

Figure 3. Critical Parameters for Calculating  $J_{IC}$  from Load-displacement Curves.

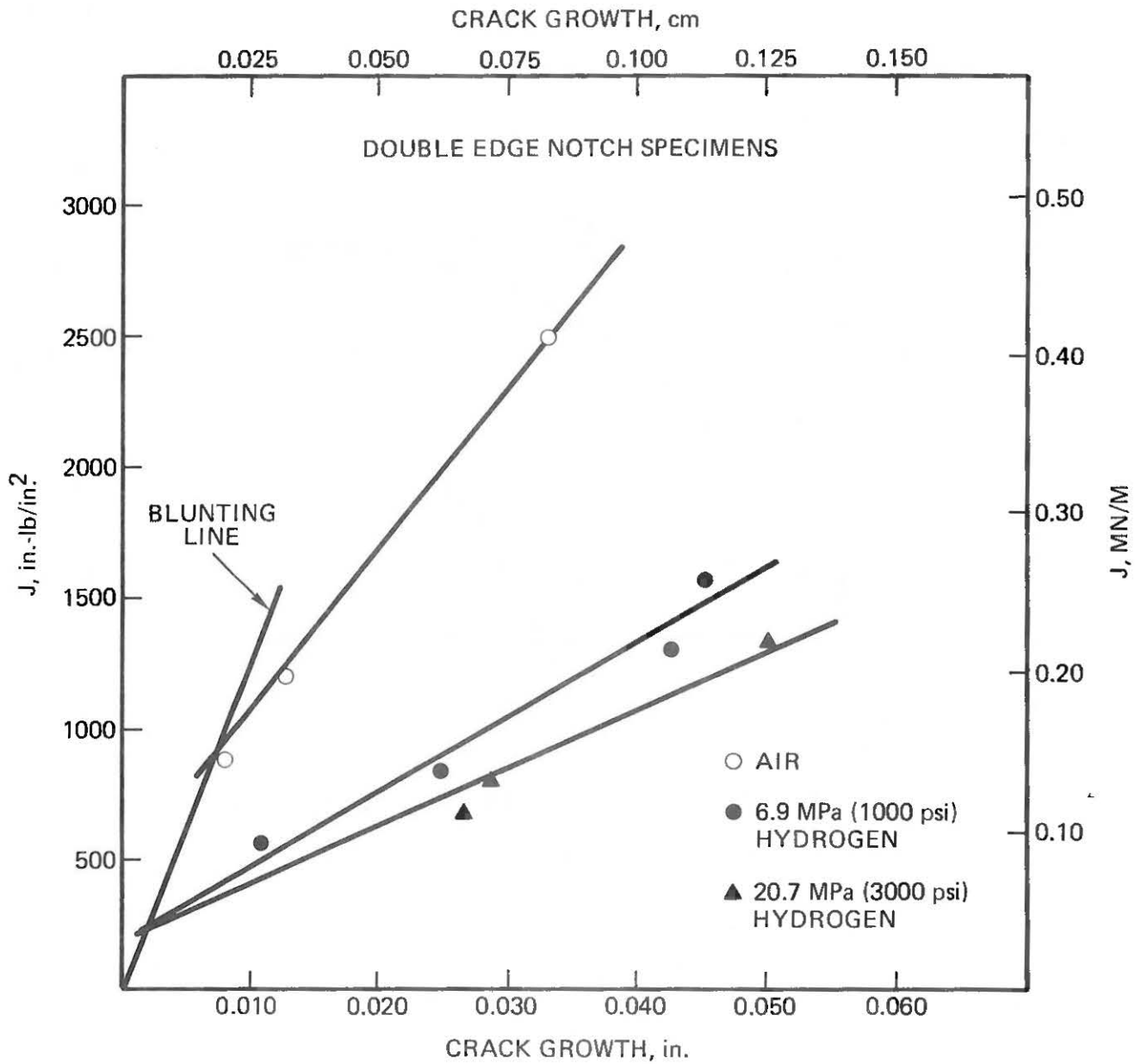


Figure 4. Energy for Crack Extension, J vs. Crack Growth.

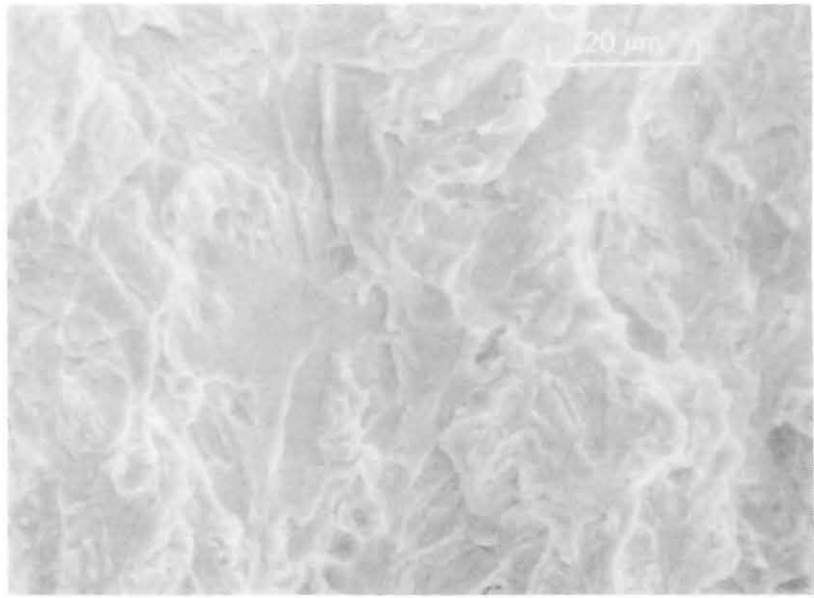


a

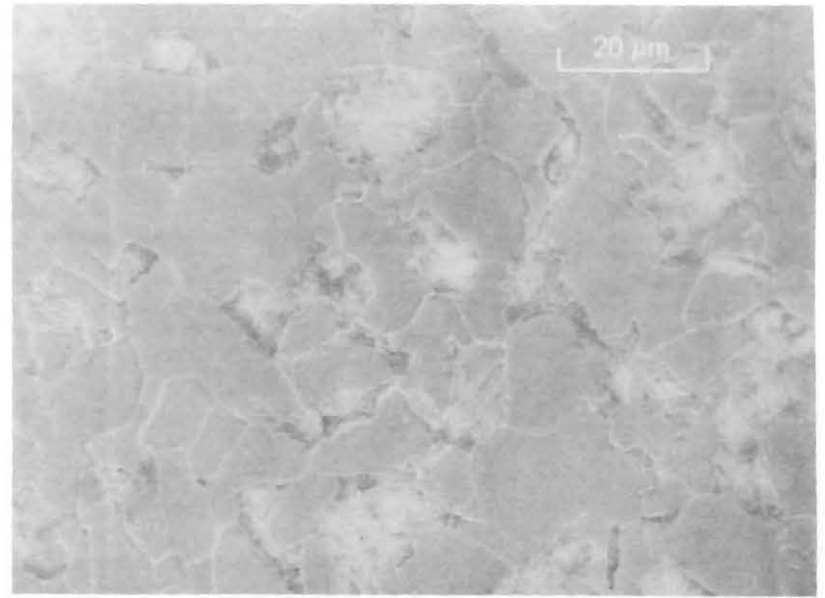


b

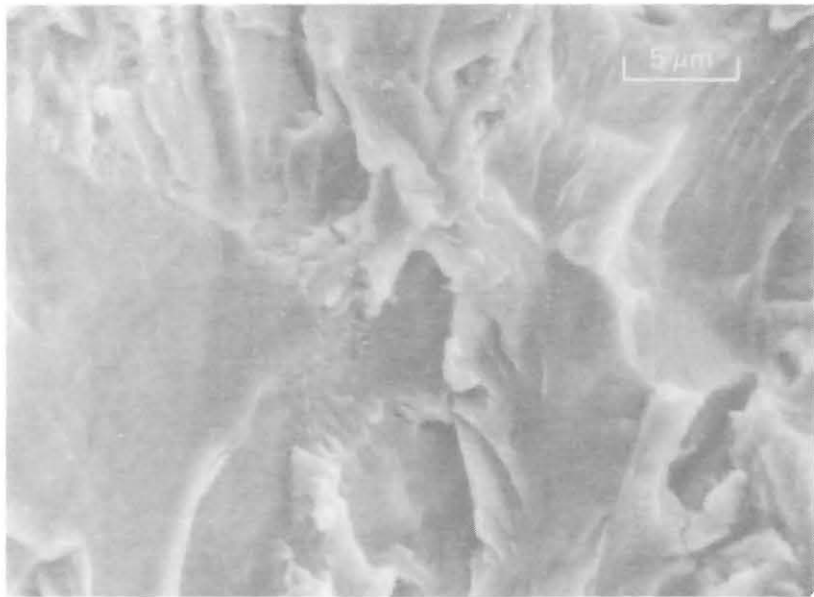
Figure 5. Fracture Surfaces of A516 Tested in Air, (a) Fracture Features, (b) Comparison Microstructure.



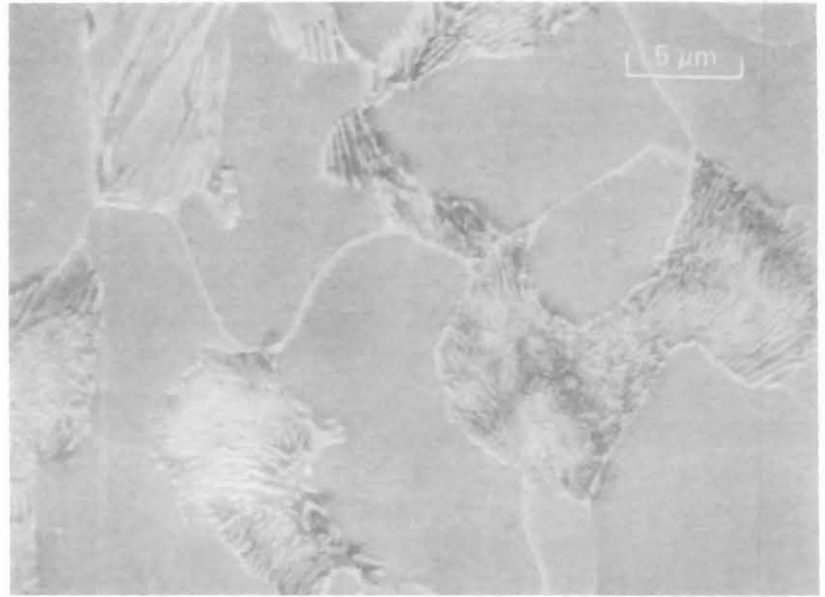
a



b

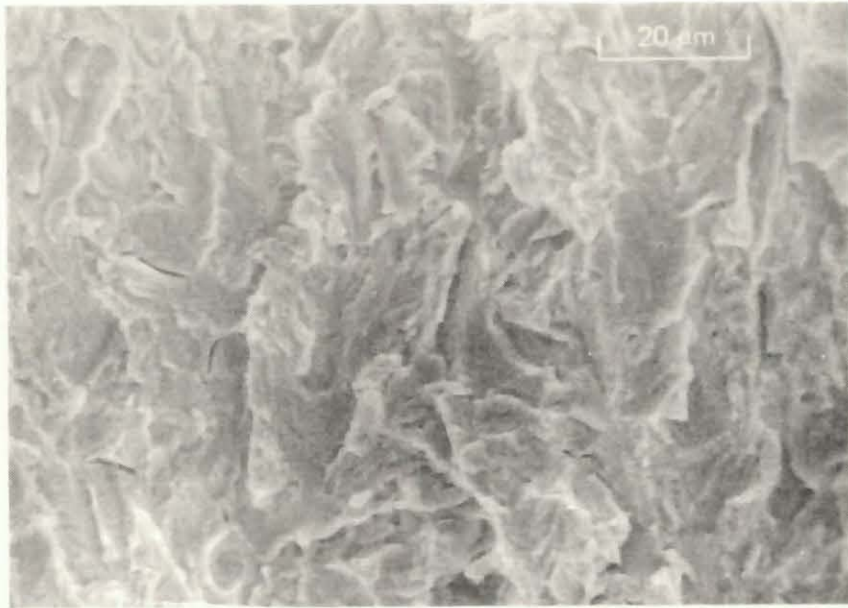


c

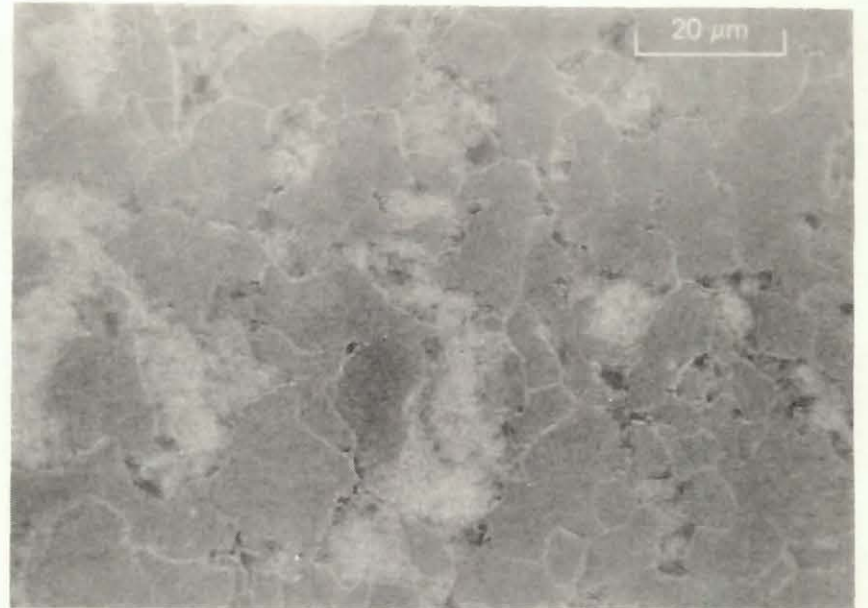


d

Figure 6. Fracture Surfaces of A516 in 1000 psi Hydrogen, (a) and (c), Fracture Features (b) and (d) Comparison Microstructure.



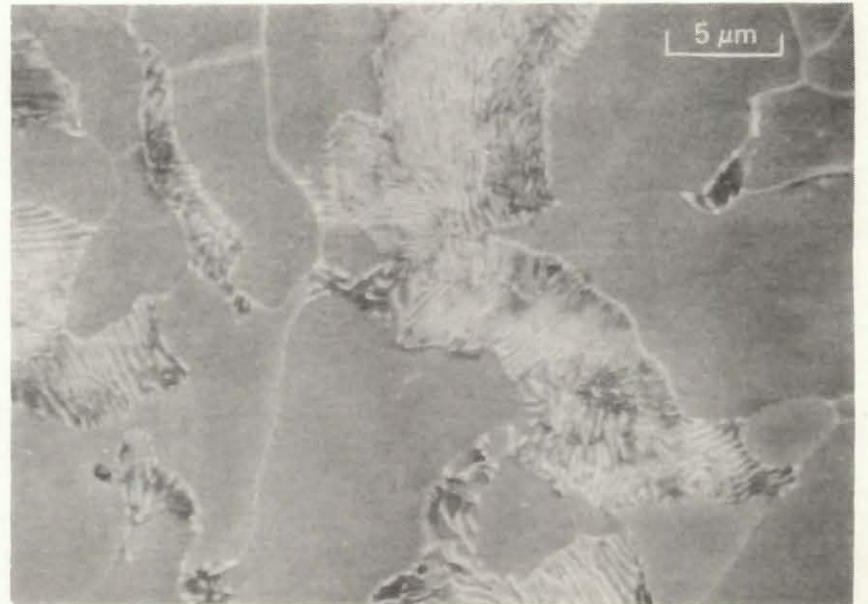
a



b



c



d

Figure 7. Fracture Surfaces of A516 in 3000 psi Hydrogen, (a) and (c), Fracture Features (b) and (d) Comparison Microstructure.

## REFERENCES

1. W. R. Hoover, "Hydrogen Compatibility of Structural Materials for Energy Storage and Transmission," SAND79-8200, 1979, p. 47.
2. J. P. Hickerson, Jr., Eng. Fracture Mechanics, 9, 1977, p. 75.
3. W. F. Brown, Jr. and J. E. Srawley, ASTM STP No. 410, ASTM, 1969, p. 39.
4. H. G. Nelson, On the Mechanisms of Hydrogen-Enhanced Crack Growth in Ferritic Steels, in Proceedings, 2nd Int. Conf. on Mech. Behavior of Materials, ASM, Boston, 1976, p. 690.
5. W. G. Clark, Jr., "Effects of Temperature and Pressure on Hydrogen Cracking in High Strength Type 4340 Steels, J. Matls. for Energy Systems, 1, 1979, p. 33.
6. M. R. Shanabarger, " Chemisorption Kinetics of Hydrogen on Evaporated Iron Films," Surface Science, 52, 1975 p. 689.
7. J. K. Tien, A. W. Thompson, I. M. Bernstein and R. J. Richards, "Hydrogen Transport by Dislocations," Met. Trans. 7A, 1976, p. 821.
8. H. H. Johnson, in "Hydrogen in Metals," I. M. Bernstein and A. W. Thompson, Eds. ASM, 1974, p. 35.
9. M. R. Louthan, VPI, private communication, 1979.
10. C. D. Beacham, "A New Model for Hydrogen Assisted Cracking (Hydrogen "Embrittlement"). Met. Trans. 3, 1972, p. 259.
11. H. Birnbaum, U. of Illinois, private communication, 1979.

## V. Hydrogen Embrittlement of Pipeline Weldments

J. R. Spingarn

### Introduction

Any evaluation of the feasibility of transporting gaseous hydrogen through the natural gas pipeline system must consider the effects of large variations in pipe chemistry and microstructure. Since it would be impractical to investigate all possible base metal and weld microstructures, it is important to try to isolate the materials most susceptible to hydrogen embrittlement and then select safety factors with these materials in mind. In general, many investigators have found that mild steels do not display the dramatic changes in properties often associated with hydrogen effects and thus a rank ordering of materials and microstructures is not a straightforward task. In this study, the uniaxial tensile test was used to try to contrast a wide variety of linepipe base metals and weldments.

The chemistries of the materials tested during the last year are listed in Table I. For all materials, except the A516-USA and A516-JAP plate steels, specimens were machined from linepipe recently removed from the ground or about to be placed in service. The pipe ranges from the conventional C-Mn compositions commonly used during the last 25 years for X42 and X50 grade linepipe, to more modern X60 through X70 grade pipe whose composition includes low alloy additions for increased strength and improved low temperature toughness. Base metal (BM) specimens were oriented parallel to the rolling direction, while seam weld (SW) and girth weld (GW) specimens were cut perpendicular to the weld. It is assumed that the materials and weld practice for all the pipe studied met the specifications of API 1104 appropriate to the time of pipe installation. The mechanical properties of these specimens do not always agree with reported values on similar material for two reasons: (1) reverse bending was sometimes necessary in order to machine the tensile bars, and (2) subsize specimens were used (as illustrated in Table II, different diameter specimens show significant variations in ductility). For pipe diameters smaller than 3/16 inch only a subsize specimen could be obtained, thus in order to test all materials on an equal basis, a small test specimen was selected. The tests were all carried out at an extension rate of 0.02 inches/minute in a high pressure H<sub>2</sub> test cell. Tests were conducted in either air or 6.9 MPa high purity H<sub>2</sub>. In order to overlay mechanical test results and match machine compliance, all experiments were conducted on the same testing machine. The microstructures of the base metals and weldments were illustrated in the previous report.<sup>(1)</sup>

## Results and Discussion

The test results are summarized in Tables II-VIII. Each reported value represents the average of two specimens. The data scatter was generally within 2% of the reported average, and thus strength differences of 1-2 ksi are not considered significant. Weld specimens with obvious macroscopic defects were discarded. From the smooth bar tensile tests two broad conclusions can be drawn. (1) The presence of the external H<sub>2</sub> environment has negligible effect on yield strength and UTS for all base metal chemistries and weld metal microstructures. (2) The ductilities as measured by percentage reduction in area (RA) in H<sub>2</sub>, for all the linepipe tested were virtually the same (Figure 1). With the exception of A106-BM which showed unusually high RA in H<sub>2</sub>, and ARC-GW where weld defects were apparent on the fracture surface, the remaining materials (including both base metal and weldment microstructures) retained approximately 35% smooth bar reduction in area in H<sub>2</sub>. This corresponds to about a 50% RA loss due to the hydrogen environment. There were regions of H<sub>2</sub>-induced surface cracking on all specimens, however as typified by the stress-strain curve shown in Figure 2, the H<sub>2</sub> effects do not appear significant until after the UTS is reached. Indeed, it is generally observed that specimen necking develops at strains beyond the UTS, and our results strongly indicate that the branching of the air and H<sub>2</sub> stress-strain curves does not occur until strains larger than the UTS. Thus the cracking and H<sub>2</sub>-induced ductility loss are clearly tied to the localization of flow at the specimen neck.

Since the effects of H<sub>2</sub> become most pronounced when the stress and strain are localized, as during necking, the notched bar tensile test is a more sensitive measure of hydrogen embrittlement than the smooth bar test. Notched bar tensile test results are also presented in Tables II-VIII, where the reported stresses are based on the minimum area at the notch, and tensile ductilities are based on inches of extension, as well as % RA. Representative stress-elongation curves are shown in Figures 3-5. Using interrupted tensile tests it was found that in the gaseous hydrogen environment, the specimens are unaffected by the H<sub>2</sub> until surface cracks develop, and from that point the cracks grow and fracture follows. The point at which cracks begin to grow coincides with the separation of the air and H<sub>2</sub> curves and corresponds closely with the load maximum for the H<sub>2</sub> specimen. The % RA values from notched specimens were presented in Figure 1. One can see that all the materials tested average 9% notched tensile RA in H<sub>2</sub>, for the specific geometry studied in these tests. Again, the ductility was found to be insensitive to the chemistry or microstructure of any material.

It is clear from the tables that the high strength steels tested will tolerate very little localized strain in the presence of H<sub>2</sub>. The values for the critical elongation to initiate crack growth  $\Delta\epsilon_u(H_2)$ , measured as the elongation at maximum load were correlated with a variety of tensile parameters. The quantity  $\Delta\epsilon_u(H_2)$  was found to correlate best with notch yield strength measured in hydrogen (Figure 6), while poorer correlations were found using tensile strengths, ductility and work hardening rate. In view of the large measured range of values in  $\Delta\epsilon_u(H_2)$  it can be concluded that the H<sub>2</sub> embrittlement of mild steel cannot be simply explained on the basis of localized plastic strain, or for that matter on localized stress,

since the maximum load during notched bar testing also varied considerably. The surprising conclusion that can be drawn is that the notched bar fracture initiation in H<sub>2</sub> is strongly dependent on the macroscopic plastic flow properties of the material in question, and only mildly dependent on chemistry or microstructure. This suggests that the materials and welding options for H<sub>2</sub> service are somewhat limited. Further, it can be seen that steels whose yield strengths (or tensile strengths as well, since the high strength mild steels generally have low work hardening rates) approach 100 ksi will tolerate almost no plastic strain in the presence of H<sub>2</sub>. It should be cautioned that these results are only applicable to crack initiation during rising load testing, such as monotonic tensile testing, burst testing and rising load fracture toughness testing. The insensitivity to chemistry and microstructure during H<sub>2</sub> testing may not hold true for fatigue cycling or sustained load cracking. Additional work needs to be conducted along these lines.

The effect of H<sub>2</sub> on crack propagation during uniaxial tensile testing is more difficult to describe due to the restrictions imposed by testing small specimens. It was found that the extent of H<sub>2</sub>-induced flat fracture (a macroscopic description of quasi-cleavage) varied significantly from material to material, as illustrated in Figure 7. The depth of H<sub>2</sub>-induced crack penetration ranged from almost none for A516-BM to almost 100% for A106-GW. This penetration depth does not correlate well with any of the smooth or notched bar tensile properties, but can generally be predicted from the amount of post-necking strain and the final fracture stress. The greater the post-necking strain and the smaller the final fracture stress, the greater the extent of H<sub>2</sub>-induced flat fracture as might be expected (except for materials for which virtually no flat fracture is observed).

The entire crack growth process occurs during the decreasing load portion of the load-elongation curve. Thus the crack length is increasing while the stress is decreasing in a fully plastic body and it is difficult to assign any meaningful toughness values to this test. Finally, the H<sub>2</sub> cracks are entirely transgranular during constant crosshead extension however there are some suggestions that the cracking may turn intergranular during load relaxation. More tests are planned to confirm this observation.

## Conclusions

1. A wide variety of linepipe steels and weldments were tested in uniaxial tension in a gaseous 6.9 MPa hydrogen environment. The hydrogen had negligible effect on smooth bar yield and tensile strengths and notched bar yield strength. Ductilities were affected by the presence of H<sub>2</sub>, with a smooth bar RA loss of 50%, a smooth bar RA in H<sub>2</sub> averaging 35%, and a notched bar RA in H<sub>2</sub> averaging 9%.
2. The notched bar ductility degradation was found to be insensitive to chemistry and microstructure, but highly dependent on yield strength. In other words, embrittlement was dominated by plastic flow behavior, rather than microstructural features.

3. Variations in the extent of H<sub>2</sub> crack penetration have been observed and attempts will be made to correlate these variations with upcoming fracture toughness tests.

#### Future Work

The emphasis in our future work has shifted to fracture toughness studies of pipeline weldments and higher strength pipeline steels. To accomplish this we have obtained a high strength low alloy (X60 grade) pipeline steel from Kaiser Steel Corporation. One lot of material contains a single submerged arc weld, while a second lot contains two submerged arc passes on opposite sides of the plate. The weld conditions closely approximate those employed during linepipe seam welding. These specimen plates will permit us to measure J-integral toughness values for both tempered and untempered material. The welded plates are currently in-house and have successfully passed radiographic inspection.

TABLE I  
BASE METAL CHEMISTRY

	C	Mn	P	S	Si	V	Cb	Ag	Cu	Ni	Mo
A516-USA	.21	1.04	.012	.020	.21						
A516-JAP	.26	.79	.013	.033	.17						
A106-B (typ.)	<.30	.3-1.06			>.10						
A14	.11	1.44	.013	.002	.27	.090	.040	.037	.29	.27	
EXPTL. ARCTIC	.06	1.70	.010	.009	.20		.062				.30
BF 5	.22	1.23			.11		.020				
DG 2	.14	.98	.015	.012	.29		<.01	<.012			
AG 3	.26	1.39	.006	.022	.03	.050					

TABLE II

## A516

		$\sigma_{.2\%}^{**}$	UTS	$e_u$	$e_{TOT}$	%RA
(a) A516-USA <sup>†</sup>						
Smooth <sup>*</sup>	Air	54.4	77.6	12.4	17.1	69.5
Smooth	H <sub>2</sub>	52.8	79.8	14.9	19.5	43.1
Notch <sup>***</sup>	Air	74.6	110.0	.036"	.050"	29.6
Notch	H <sub>2</sub>	78.4	91.1	.010"	.013"	5.4
(b) A516-JAP						
Smooth <sup>*</sup>	Air	52.7	82.0	14.0	21.8	72.0
Smooth	H <sub>2</sub>	52.1	82.8	13.9	18.3	37.0
(c) A516-JAP						
Smooth <sup>††</sup>	Air	54.6	78.2	18.4	25.0	71.0
Smooth	H <sub>2</sub>	54.0	77.8	18.0	24.4	46.2

<sup>†</sup>Reported results are average of two tests

<sup>\*</sup>Specimen diameter = 0.113 inch

<sup>\*\*</sup>Notch yield stress equals stress at .001 inch plastic elongation

<sup>\*\*\*</sup>Notch geometry: 90° angle, .001-.002 inch root radius, Dn/Do = .85

<sup>††</sup>Specimen diameter = 0.252 inch

TABLE III  
A106 GRADE B

		$\sigma_{.2\%}$	UTS	$e_u$	$e_{TOT}$	%RA
<b>(a) Base Metal</b>						
Smooth	Air	67.0	81.0	6.6	14.0	58.2
Smooth	H <sub>2</sub>	72.9	83.5	3.9	10.8	50.0
Notch	Air	89.6	106.4	.019"	.033	25.8
Notch	H <sub>2</sub>	89.7	97.8	.008	.012	8.0
<b>(b) Girth Weld</b>						
Smooth	Air	57.0	89.2	11.3	20.9	77.2
Smooth	H <sub>2</sub>	55.8	80.2	9.4	13.6	39.9
Notch	Air	82.6	104.2	.038	.057	49.4
Notch	H <sub>2</sub>	78.4	87.4	.010	.015	14.3

TABLE IV  
A14

		$\sigma_{.2\%}$	UTS	$e_u$	$e_{TOT}$	%RA
Smooth	Air	90.7	100.5	7.3	15.8	77.0
Smooth	H <sub>2</sub>	82.1	94.7	10.8	14.5	37.3
Notch	Air	123.1	137.1	.018"	.038	45.5
Notch	H <sub>2</sub>	121.8	122.5	.002	.006	8.7

TABLE V  
EXPTL ARCTIC - GRADE

		$\sigma_{.2\%}$	UTS	$e_u$	$e_{TOT}$	%RA
<b>(a) Base Metal</b>						
Smooth	Air	101.0	106.3	6.5	14.5	77.4
Smooth	H <sub>2</sub>	100.8	106.2	6.7	12.3	37.4
Notch	Air	144.0	148.9	.008"	.025	41.8
Notch	H <sub>2</sub>	137.5	137.5	.001	.004	8.6
<b>(b) Seam Weld</b>						
Smooth	Air	94.1	99.4	5.2	12.3	69.2
Smooth	H <sub>2</sub>	93.2	98.3	5.2	9.5	36.8
Notch	Air	143.4	145.2	.006	.012	35.0
Notch	H <sub>2</sub>	141.0	141.0	.001	.004	10.0
<b>(c) Girth Weld</b>						
Smooth	Air	79.8	97.6	7.0	14.5	80.0
Smooth	H <sub>2</sub>	86.3	88.6	0.8	1.6	16.2
Notch	Air	130.8	148.5	.012"	.018	20.5
Notch	H <sub>2</sub>	128.7	130.6	.002	.004	9.0

TABLE VI  
BF 5

		$\sigma_{.2\%}$	UTS	$e_u$	$e_{TOT}$	%RA
<b>(a) Base Metal</b>						
Smooth	Air	73.1	87.7	10.5	15.5	56.7
Smooth	H <sub>2</sub>	73.3	88.6	11.0	14.9	36.0
Notch	Air	105.6	116.8	.009"	.012	21.0
Notch	H <sub>2</sub>	106.8	109.9	.003	.004	6.1
<b>(b) Seam Weld</b>						
Smooth	Air	74.8	91.7	7.7	12.8	55.6
Smooth	H <sub>2</sub>	73.2	90.5	8.6	10.2	30.5

TABLE VII

DG 2

		$\sigma_{.2\%}$	UTS	$e_u$	$e_{TOT}$	%RA
<b>(a) Base Metal</b>						
Smooth	Air	60.0	88.3	13.1	18.6	60.5
Smooth	H <sub>2</sub>	62.2	86.6	12.0	15.1	37.1
Notch	Air	98.7	118.5	.015"	.018	15.5
Notch	H <sub>2</sub>	93.7	102.5	.005	.006	7.0
<b>(b) Seam Weld - ERW</b>						
Smooth	Air	74.4	91.7	7.0	10.0	40.0
Smooth	H <sub>2</sub>	72.3	90.0	5.6	6.1	20.4

TABLE VIII

AG 3

		$\sigma_{.2\%}$	UTS	$e_u$	$e_{TOT}$	%RA
<b>(a) Base Metal</b>						
Smooth	Air	61.9	86.1	8.7	13.0	49.2
Smooth	H <sub>2</sub>	61.1	85.5	8.1	10.0	26.6
Notch	Air	100.7	122.8	.023"	.030	22.8
Notch	H <sub>2</sub>	101.1	113.3	.008	.010	8.4

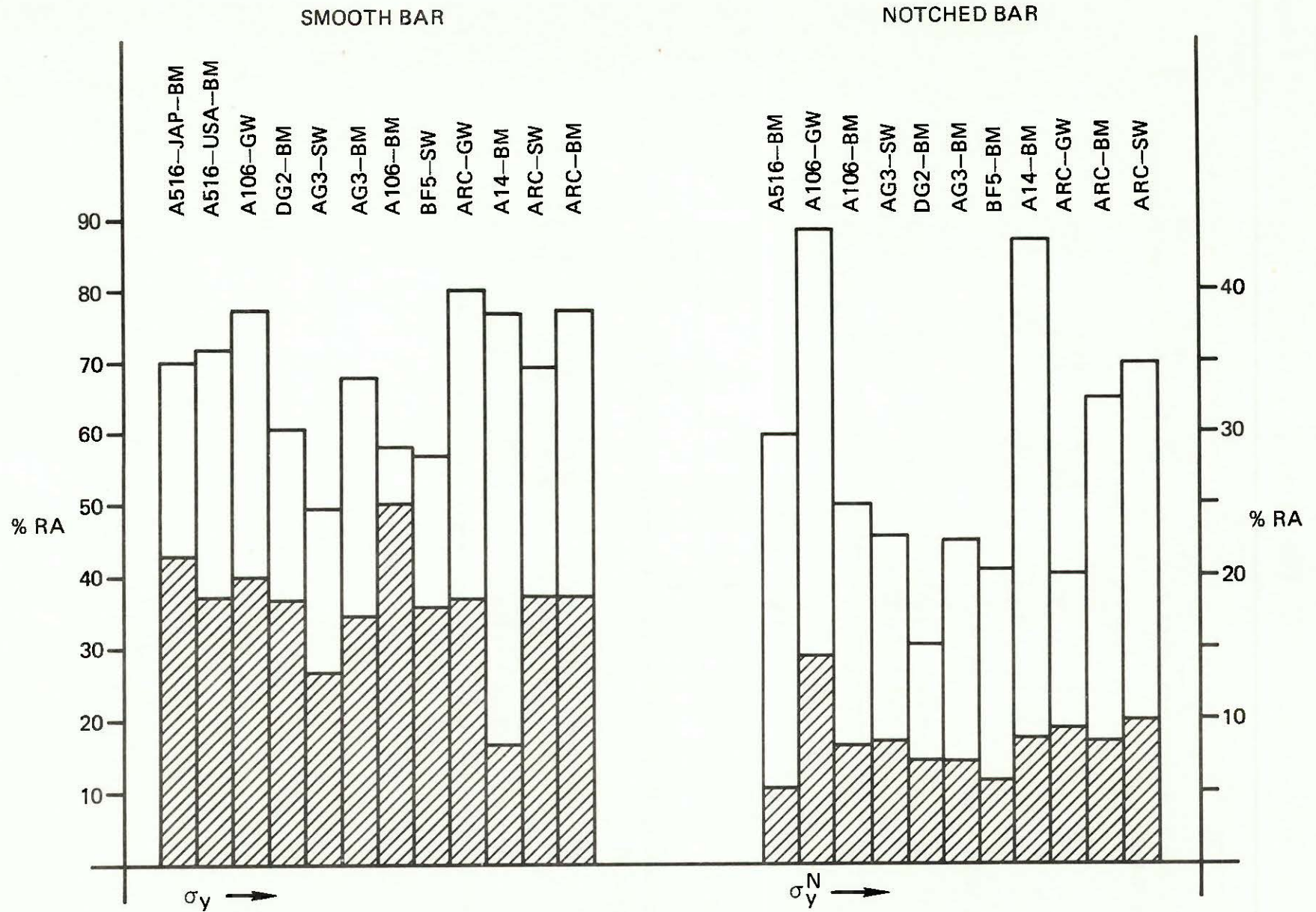


Figure 1. Ductility losses due to external hydrogen environment. Reductions in area (RA) for tests in 6.9 MPa  $H_2$  are shown hatched, while air ductilities are presented as solid. Materials are listed in order of increasing yield strength. No trends are evident.

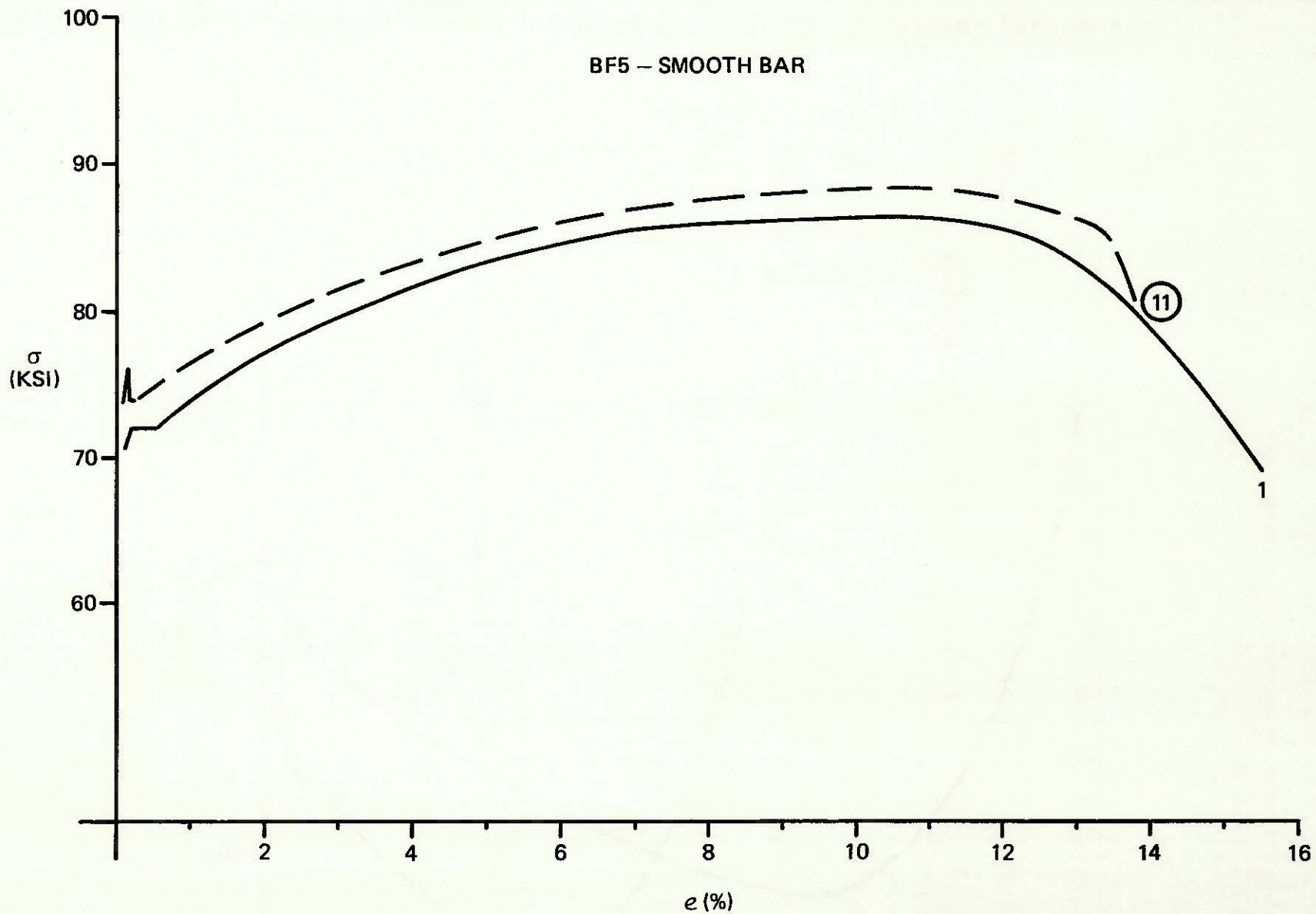


Figure 2. Stress-strain curves for smooth specimens. Circled number reflects test in H<sub>2</sub>, and uncircled number indicates test in air. Curves are similar up to point of maximum stress.

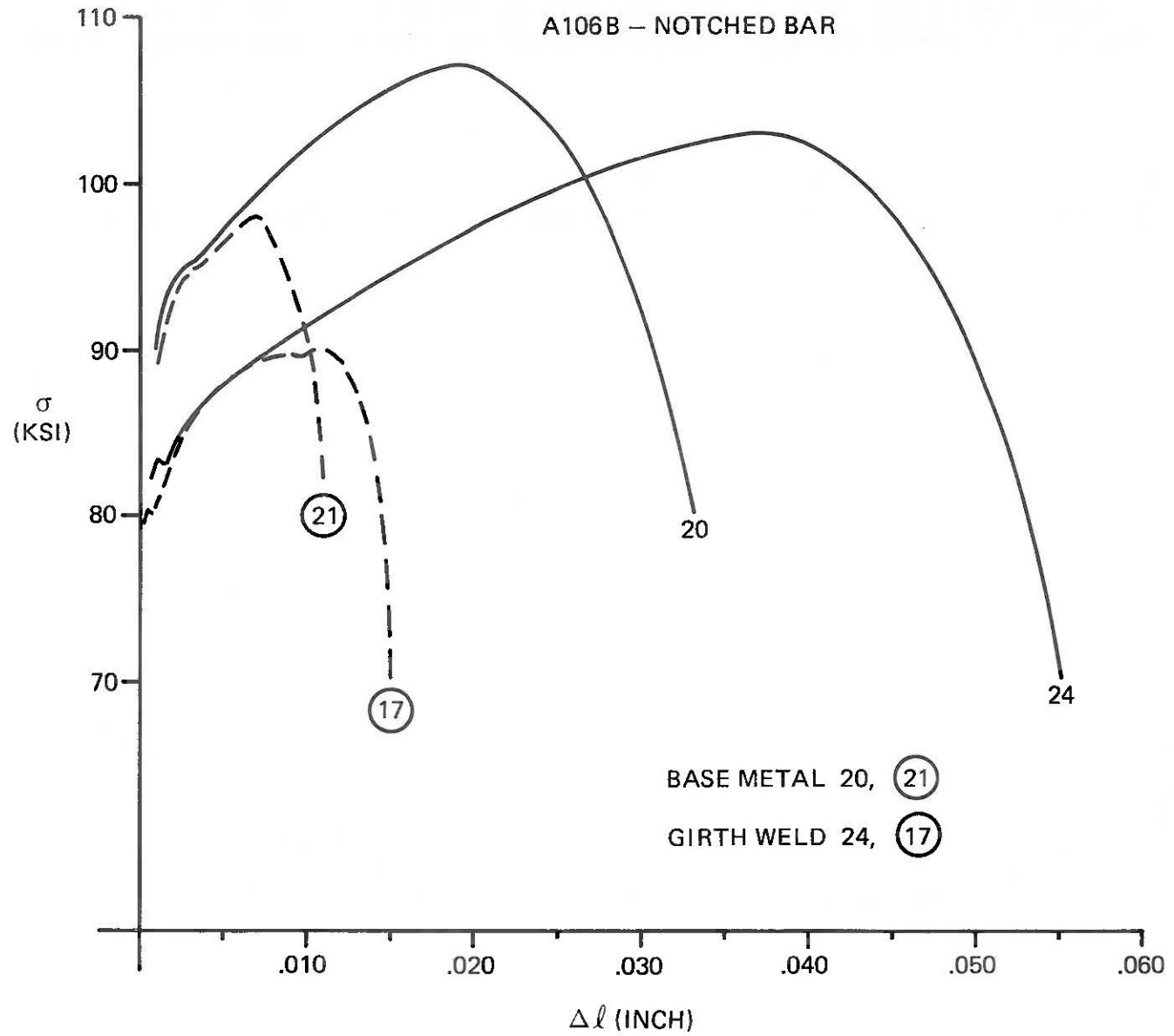


Figure 3. Stress-notch elongation curve for relatively low strength pipeline steel.

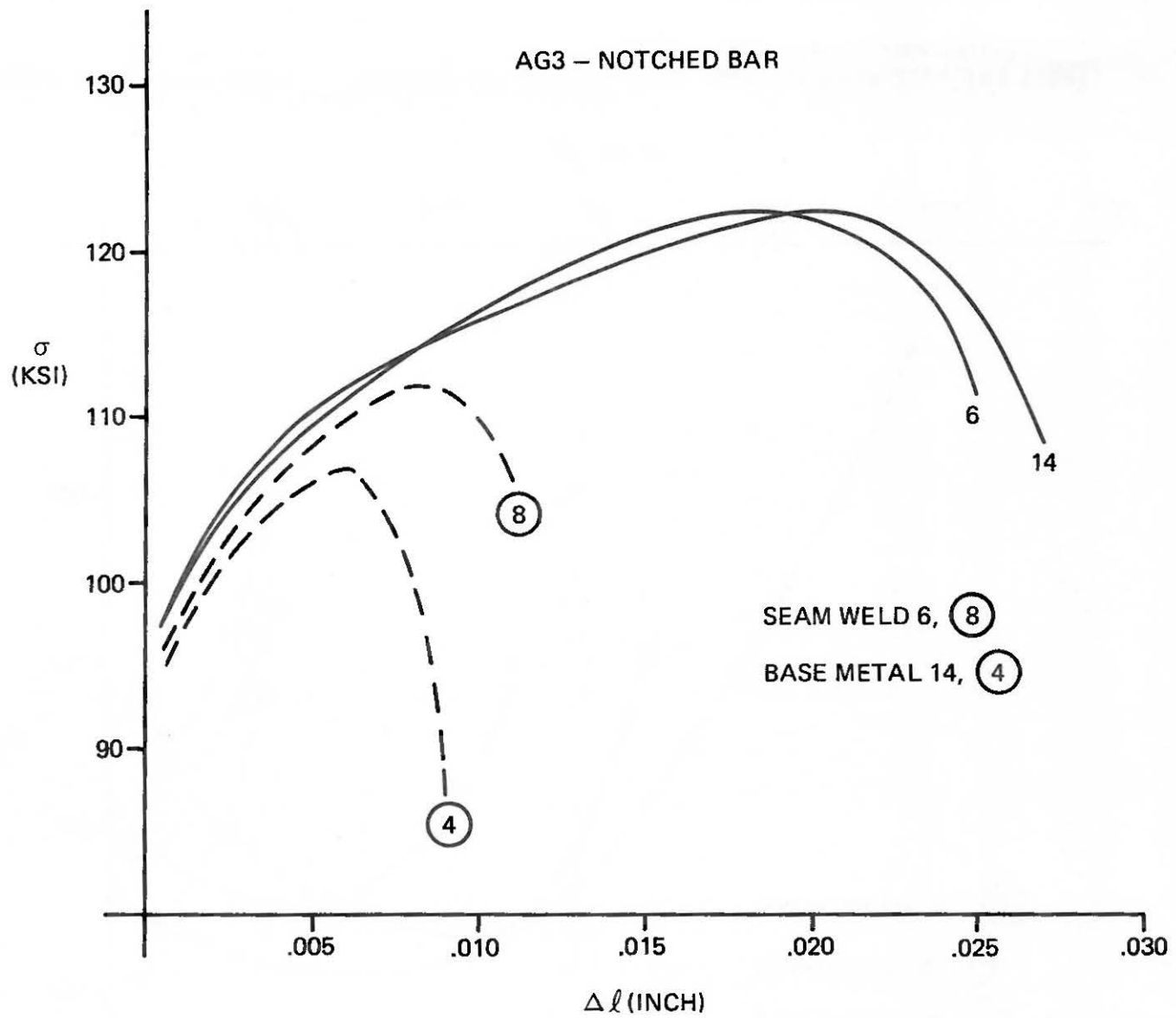


Figure 4. Stress-strain elongation curve for moderate strength pipeline steel.

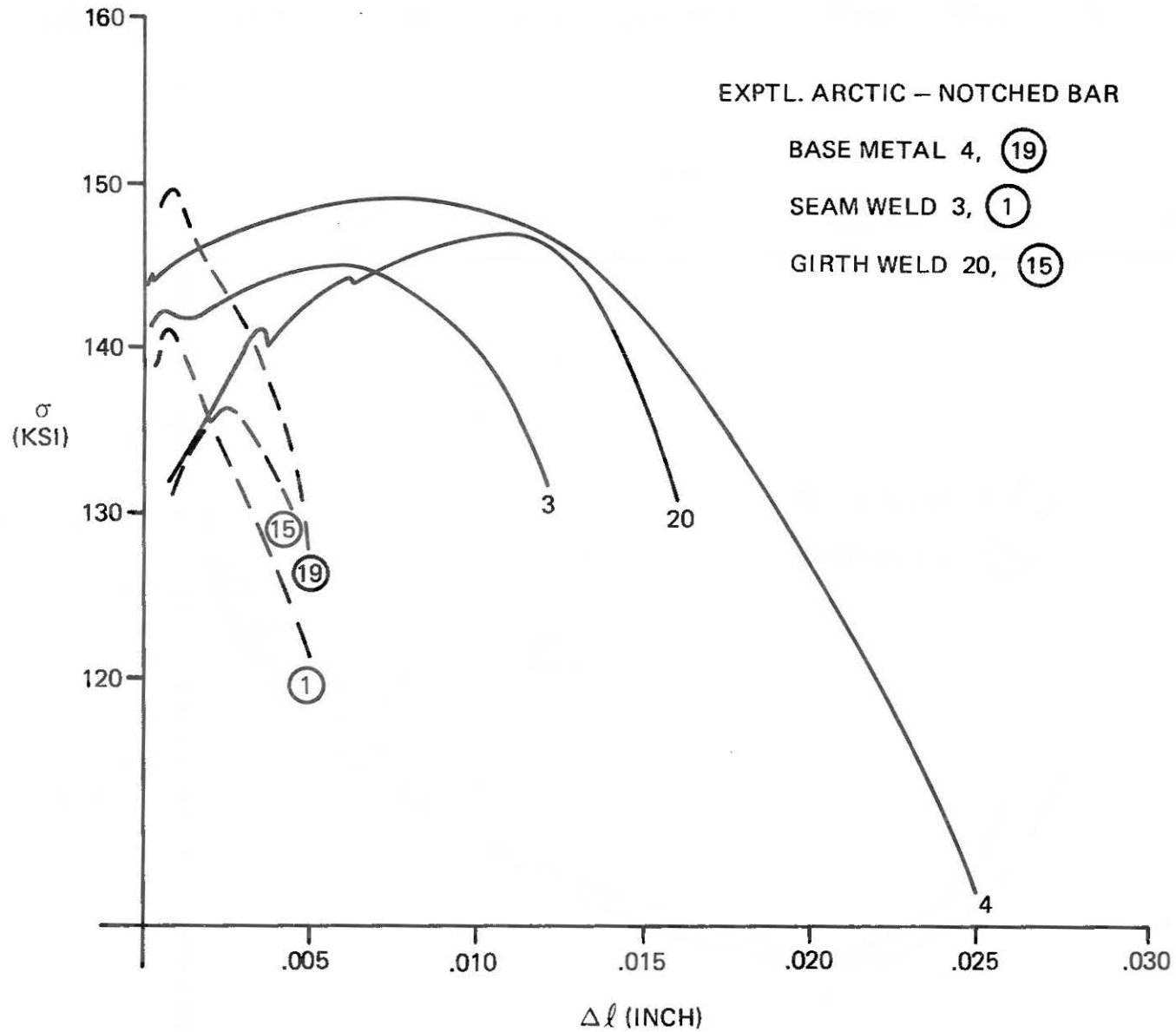


Figure 5. Stress-notch elongation for experimental high strength pipeline steel. At the highest strength levels, failure occurs almost immediately upon macroscopic yielding.

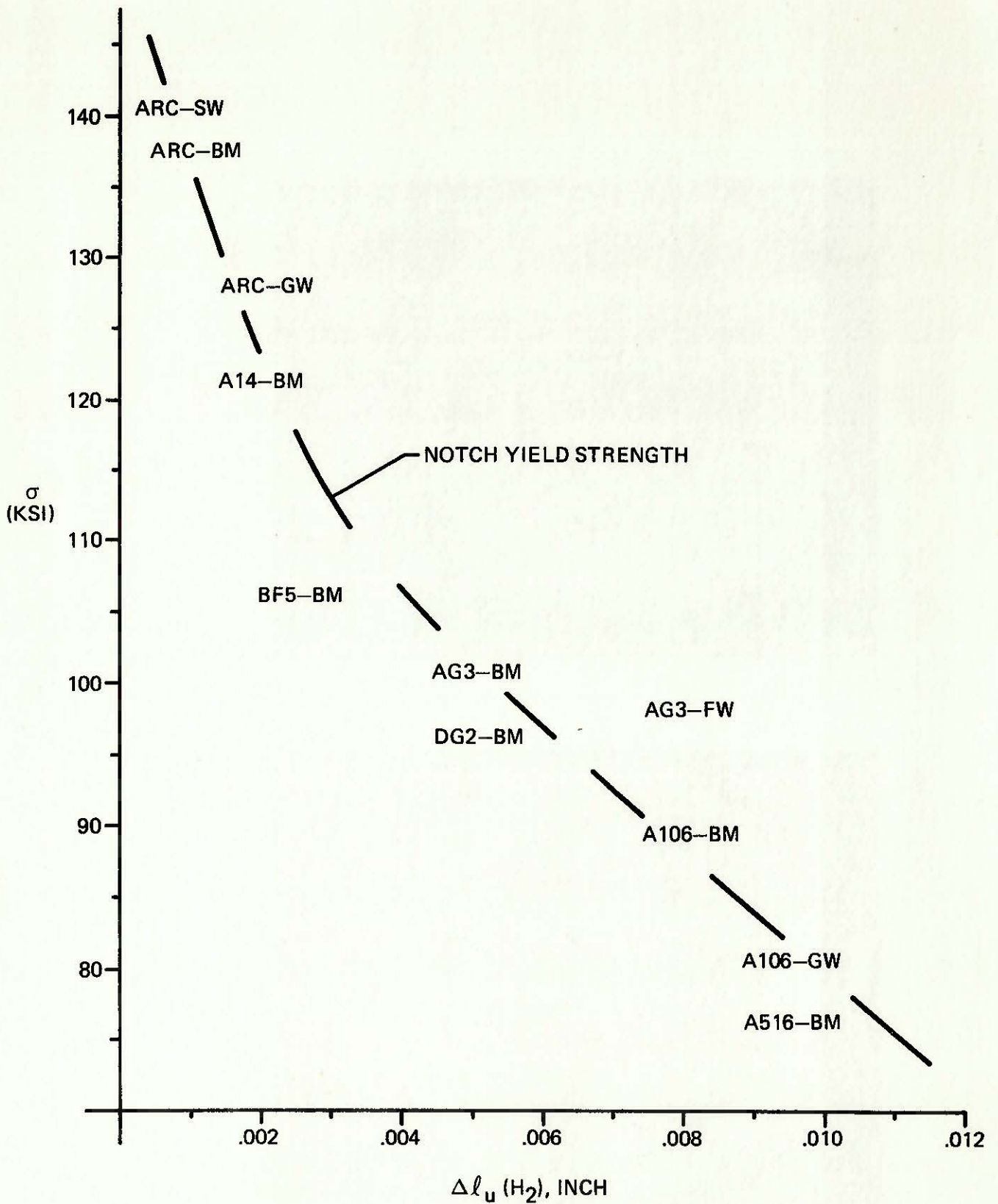
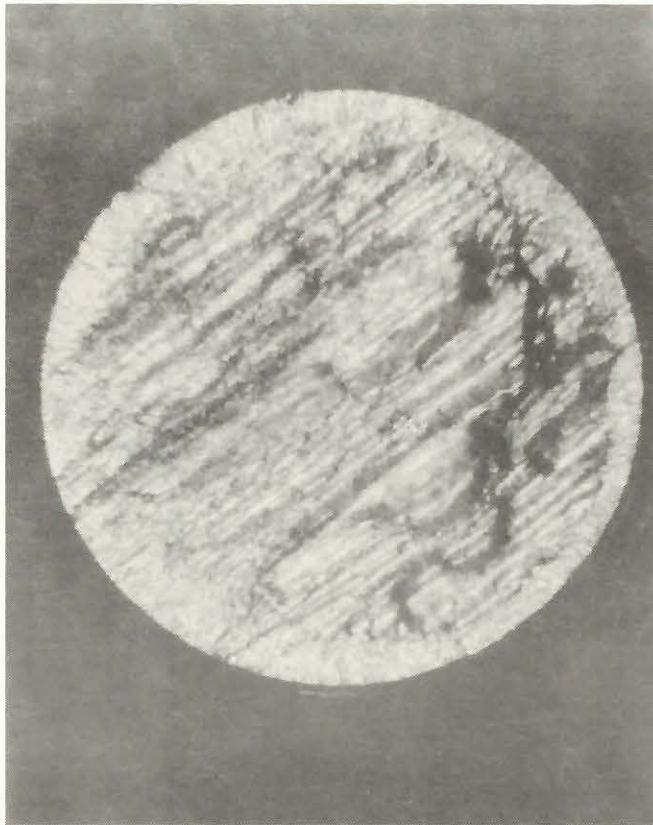
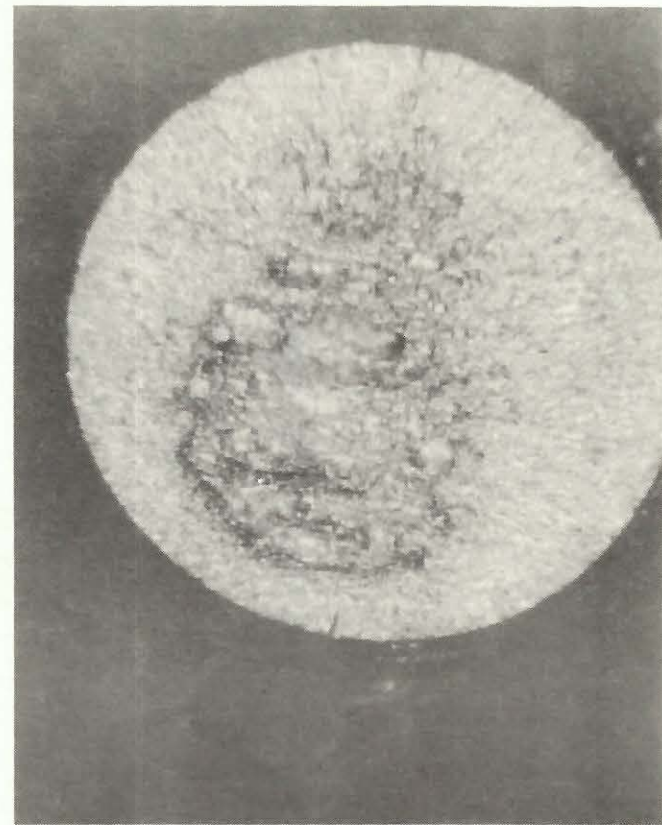


Figure 6. Correlation of notch elongation in hydrogen with measured notch yield strength. The correlation suggests that base metal chemistry and microstructure have minimal effect on notch embrittlement.

## BASE METAL FRACTURE SURFACES

800  $\mu\text{m}$ 

DG2

800  $\mu\text{m}$ 

A14

Figure 7. Variation in the extent of  $\text{H}_2$ -induced flat fracture. In general, weldments, particularly girth welds, displayed the largest crack penetration depths.

## VI. Economics of Hydrogen Storage

J. J. Iannucci and S. L. Robinson

### Introduction

Storage of hydrogen is more than simply a technical issue influenced by hydrogen embrittlement phenomena. Economics of storage is the major factor in size, location etc., and is equal in importance to safety, reliability and availability. The question of scale or amount stored relates heavily to economics and to the decision: to store or not to store. The problem has been naturally divided into two parts. First we consider the national scale of bulk storage, as would be necessary to emulate or replace the national gas supplies. Secondly, we consider a smaller scale, which might relate to energy storage for fuel applications, or chemical commodity uses. Possible trade-offs are discussed, costs developed, and possible research avenues pointed out. Throughout, we are discussing only stationary storage of hydrogen; this discussion is not pertinent to mobile applications.

### Bulk Hydrogen Fixed Site Storage Analysis

For hydrogen to play an important role in our energy future, all aspects of its usage scenario must be examined and understood. Certainly hydrogen production, transport, and end use are crucial areas for investigation, but what of storage? Widespread utilization of hydrogen may depend on the ability to store appreciable quantities to smooth mismatches between supply and demand. Storage of hydrogen may present special materials challenges due to hydrogen embrittlement phenomena and hydrogen's low heat content, which may lead to different trade-offs in storage design and performance than occur with natural gas. The necessity, viability and preliminary economics of bulk hydrogen storage are examined in this paper.

It has been assumed in this work that (1) hydrogen will be plentiful and available in all regions of the country; (2) the widest possible usage of hydrogen will be as a substantial replacement for natural gas in heating and electrical generation applications by distribution through existing natural gas pipelines and/or a similar pipeline system. Feedstock applications are also examined.

Storage of hydrogen (as with any fuel) will only be desirable if there are mismatches between production, distribution and usage rates. While this is true for any energy commodity, it is especially true for hydrogen, as it is neither a source of energy nor a necessary element in any envisioned energy economy. However, it may be an attractive medium of energy transport,

distribution, end-use, etc. Hydrogen will be produced as a gas. Storage of gaseous fuels is usually unattractive; however, there may be instances when the storage of hydrogen would be beneficial and perhaps necessary. Consider the examples of oil or natural gas--these are produced at a constant rate, not at the convenience of a utility company as hydrogen might. It may be cheaper to transmit hydrogen at the maximum production rate, rather than to store it to smooth the flow rate. Alternatively it might be better to adjust the production rate to match the instantaneous transmission capacity. At any rate, avoidance of storage at the production site may be a viable possibility. It may even be possible to avoid storage of hydrogen at a distribution site by adjusting production rates to match the actual or predicted consumption rates. This concept of storage avoidance is not an attempt to skirt the issue but rather to get to the heart of the matter; hydrogen storage is expensive in any form (as is the storage of any gas), and industry will avoid its storage whenever economically or operationally possible. The necessity of hydrogen storage is herein examined by investigating likely sources and patterns of hydrogen production, distribution limitations and end-use consumption scenarios. To determine the needs and characteristics of hydrogen storage, the hydrogen energy cycle was broken into three sectors: production, distribution, and end use. In each of these sectors storage of hydrogen may be beneficial towards smooth and economical operation.

Hydrogen storage at constant production rate sites will not be needed (as there is no advantage to storing at all). Variable production rate locations (such as solar powered conversion plants) present a slightly different picture. Here a tradeoff exists between the cost of storage (to smooth transmission rates and hence lessen pipeline sizes and costs) versus the cost of the transmission line. For the solar hydrogen production case, storage is a more expensive option than simply oversizing the transmission lines to handle the maximum production rate. This result, of course, depends on the cost of storage and the cost and length of the transmission line, but nonetheless is quite broadly applicable. Unless extremely inexpensive storage is available (less than 100\$/MBTU, 1972 dollars) or the length of the line is extremely long (say, more than 100 miles), storage is not the preferred option. In Figure 1 the breakeven distance is plotted for available storage options versus distance to transmission lines. The case of using off peak electricity for electrolysis is very similar to the solar case and for similar reasons storage is not attractive here either.

Hydrogen storage is most important and beneficial at distribution sites. This storage will be seasonal in nature (as natural gas storage is used currently). Even accounting for hydrogen's lower heating value (with respect to natural gas) the current underground natural gas storage facilities would provide almost all of the seasonal storage requirements envisioned. (Further, the amount of underground natural gas storage in the U.S. continues to increase while the consumption of gaseous fuels is decreasing.) Should this or similar storage not be acceptable for hydrogen service, the next best alternative may be above ground constructed vessels in the 1000 \$/MBTU range. Since currently  $7 \times 10^9$  MBTU of natural gas storage is used, a rough estimate of the cost of above ground hydrogen storage would be  $7 \times 10^{12}$  (seven trillion)

dollars. This would probably be unacceptable to both hydrogen utilities and their customers. Hence effort should be put into assuring the viability of inexpensive storage, such as conversion of current natural gas facilities to hydrogen service.

Storage at the end use point is not really an issue. In a postulated scenario of widespread hydrogen usage, hydrogen will be available on demand from distribution and delivery networks as natural gas now is. Residential users will almost never be interrupted and industrial and commercial users will prefer oil as a back-up heat source rather than expensive hydrogen storage. Thus storage at the end-use point will rarely be required.

The storage requirements in a scenario of widespread hydrogen use are summarized in Table I.

In summary then, the most pressing need for hydrogen storage is not at the production point (even for intermittent production) or the end use point, but rather at distribution locations. This is consistent with current natural gas practice. Conversion of natural gas storage to hydrogen service may well provide for storage at the distribution point.

#### Small Scale Fixed Site Hydrogen Storage

The previous paragraphs addressed the national problem of bulk storage of hydrogen (location, scale and cost) in a scenario of widespread usage. Small users may desire to store hydrogen, provided compatible, affordable storage modes are available. In this study, presently available and some possible future technologies are studied with the intent of identifying the minimum cost storage technique for various combinations of quantity, cycling frequency and parasitic energy costs. Peg points of 10 MWhr electric equivalent (34 MBTU), and a least-cost size scale are identified for each technology.

Three basic storage forms are considered: pressurized gas, cryogenic liquid and hydride; a fourth form, a microballoon storage is also estimated. For each form it is necessary to develop (1) installed capital cost, (2) filling and emptying equipment costs, and (3) parasitic energy consumption costs.

For storage of pressurized gas, a variety of conventional pressure vessel forms are available. These can be characterized by operating pressure; low (<500 psi), moderate (to 2000), high (2000-5000) and very high (5000-10000 psi) pressure. Those considered are, standardized API spherical and spheroidal vessels (low pressure), steel pipes (moderate pressure), and steel pressure vessels (high to very high pressures). Commercial estimates were used where possible. The question of an optimum pressure was considered. Capital cost data for pressurized storage is summarized in Figure 2 with pressure as the variable. In fact the capital cost minimum is very broad (due to the constant amount of material required to hold a given amount of gas independent of pressure). At high pressure, hydrogen embrittlement phenomena dictate rapidly increasing thicknesses with increasing pressures, to ensure safety. At some pressure (probably 3000-5000 psi) a change over to costly materials

is necessary due to embrittlement phenomena. Only the possible necessity of high pressure availability (greater than 5000 psi) could make these options attractive. Economically, low and moderate pressure storage look most attractive with installed costs below \$1500/million BTU.

Nonconventional pressure vessel technologies include (1) prestressed cast iron (PCIV) with integral liner, (2) prestressed concrete, (PCCV), (3) filament wound metal bladder, and (4) underground using overburden pressure to lessen structural requirements from the gas containing bladder. The PCIV vessel is not as economical as some of the conventional vessels, but appears to approach competitive costs in large sizes. Its inherent safety is attractive. The PCCV vessel appears to have a pressure optimum and scales well to large sizes. It has a low pressure cost minimum which appears competitive with conventional vessels; its safety may be a question mark. Fiberglass wound metal bladders were uncompetitive; replacing an inexpensive material with one more expensive (per unit load carrying ability) could not be otherwise. Burial of pressure vessels is also uneconomical, due to the costs of underground construction; great depths are required for significant structural contributions from the overburden. Optimistic costs have been developed by some authors for drilling in bedrock, etc., but these are site-specific.

The installed capital costs of cryogenic hydrogen storage are developed, and seen to be attractive (<\$75/MBTU) for large scale storage; at small sizes the cost in \$/MBTU is near that for gas storage, about \$1400/MBTU. Hydride storage capital costs approach \$3400/MBTU, because of the high price of hydride and the volume, plus the necessity of a pressure vessel. Microballoon storage has the lowest vessel capital cost, current estimates being in the \$18-32/MBTU range. This microballoon vessel cost is deceptively small however, as a facility must be built to fill the spheres. This cost is included later in the overall system costs. The filled microballoons must be stored somewhere, albeit at ambient temperature and pressure and it is this small cost that is shown.

Single cycle parasitic energy costs are determined: pressurization costs, liquefaction costs, combined heat and pressure for the microballoon system all where developed and applied to the appropriate system. Cycling requirements (daily, weekly and seasonal) were added to the above costing data. Using two scales, the 34 MBTU and optimum size, the total cost (installed capital plus parasitic energy (present valued) plus cycling requirements) was calculated using electric rates as a parameter. The results are graphically shown in Figures 3 through 8, and summarized below. The specific conditions used for the comparisons shown in the figures are listed in Table II.

For either the 34 MBTU or the optimum scale, energy intensive systems such as liquefaction or microballoons, fared poorly for daily cycling. Low pressure storage was the most economical technique, with costs ranging from 1200 \$/MBTU (present value) depending upon energy costs. For weekly cycling, a complex mix developed dependent upon energy costs. For seasonal cycling, the energy intensive, low capital cost systems, were superior in large sizes; for small (34 MBTU) quantities microballoon storage appeared to be superior (less than \$100/MBTU) with low pressure and liquefaction storage costing \$1100-1500/MBTU. The costs obtained are estimates, and indicated clear choices for large seasonal, and both large and small daily cycling. Several choices are viable for the other duty cycles. While microballoon storage estimates are rough, this technology does look promising.

The complete text of these reports is available as Sandia reports, Applications Analysis of fixed Site Hydrogen Storage, SAND78-8272, J. J. Iannucci and S. L. Robinson, and Technologies and Economics of Small Scale Hydrogen Storage, SAND79-8646, S. L. Robinson and J. J. Iannucci.

TABLE I  
SUMMARY OF STORAGE REQUIREMENTS

Application	Storage Requirements
Continuous Production Point	None
Intermittent Production Point	Cavern Storage Viable Only
Distribution Point	Current Natural Gas Technology And Capacities May Be Sufficient
End Use Point	None

TABLE II

## EXPLANATION OF STORAGE TECHNOLOGY DESIGNATORS

<u>Designator</u>	<u>Storage Design</u>	<u>Base Scale for Storage Design (MBTU)</u>
PV0	100 psi Prestressed Concrete Pressure Vessel	$\geq 70$
PV1	300 psi Prestressed Concrete	$\geq 70$
PV2	900 psi Pipe Pressure Vessel	$\geq 100$
PV3	2700 psi Welded Steel Vessel	$\geq 34$
PV4	8100 psi Superalloy Pressure Vessel	$\geq 34$
L	Liquefaction	$\geq 35,000$
H	Hydride	any
M	Microspheres (3700 psi)	any

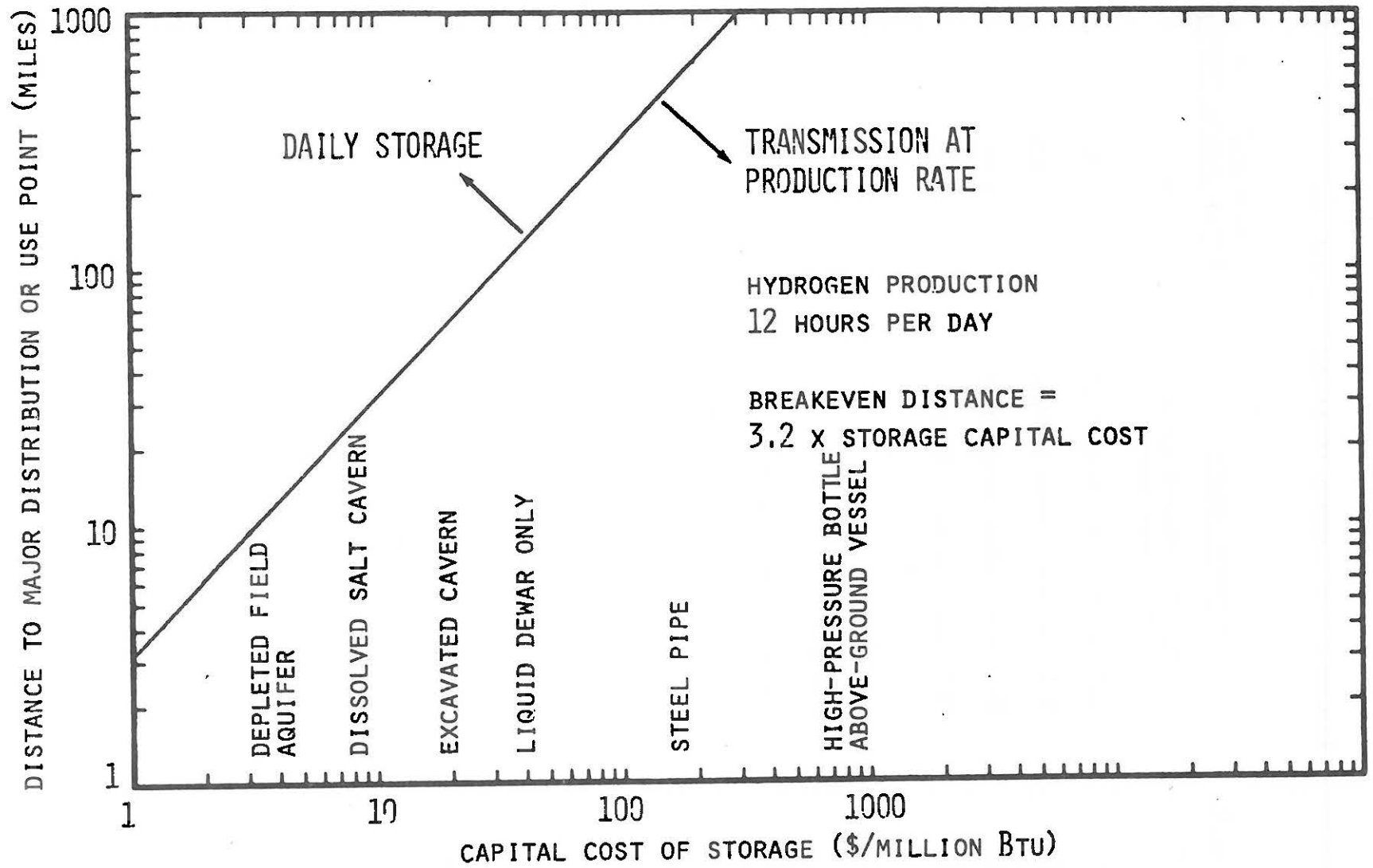


Figure 1. Breakeven Transmission Distance Versus Capital Cost of Storage for Solar Hydrogen Production.

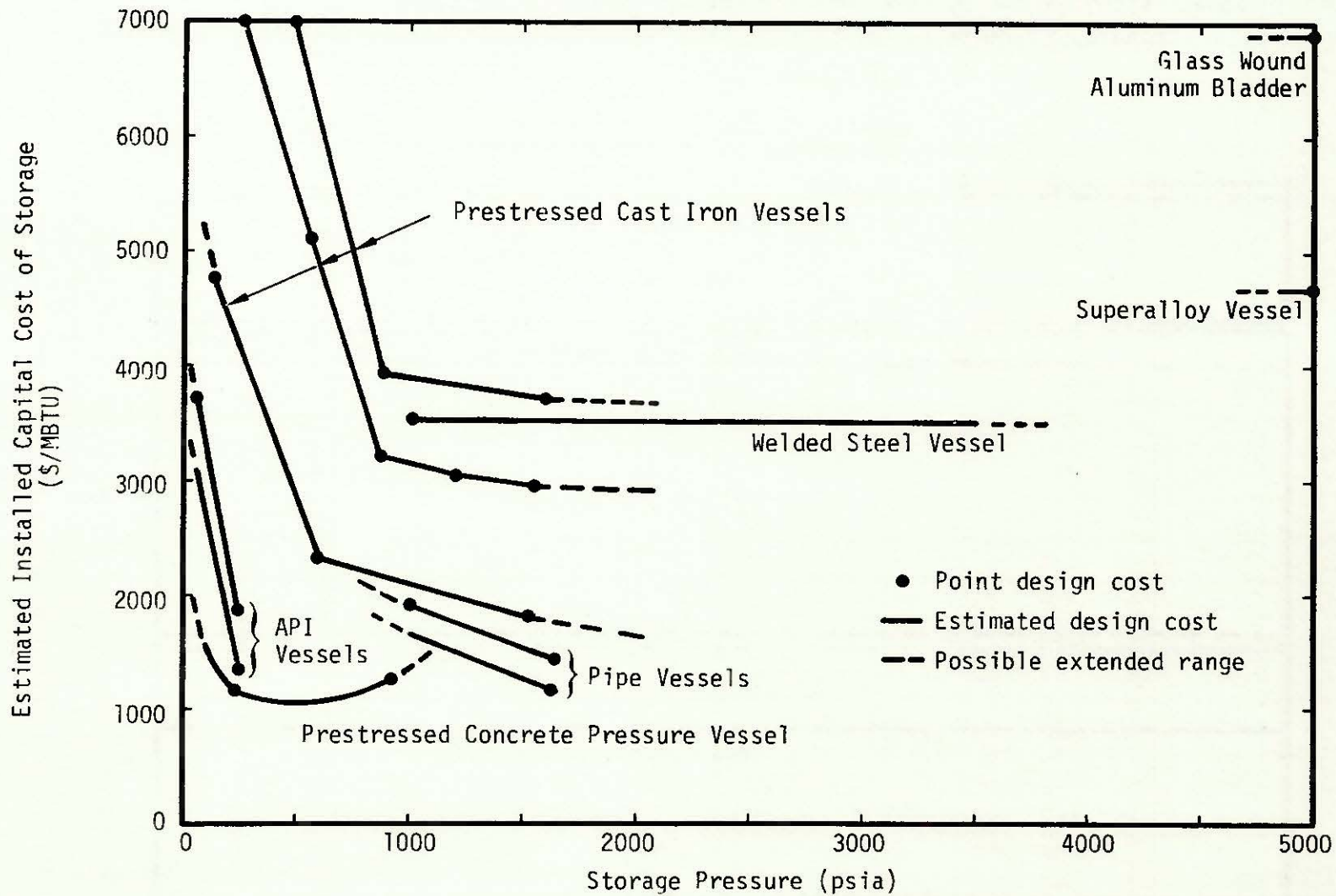


Figure 2. Estimated capital cost of pressure vessel hydrogen storage versus pressure. Error bands of  $\pm 20\%$  should be applied to each of these curves. Note that API and pipe vessel designs do not allow higher pressure extended ranges. Multiple curves for a given design are due to variation in scale.

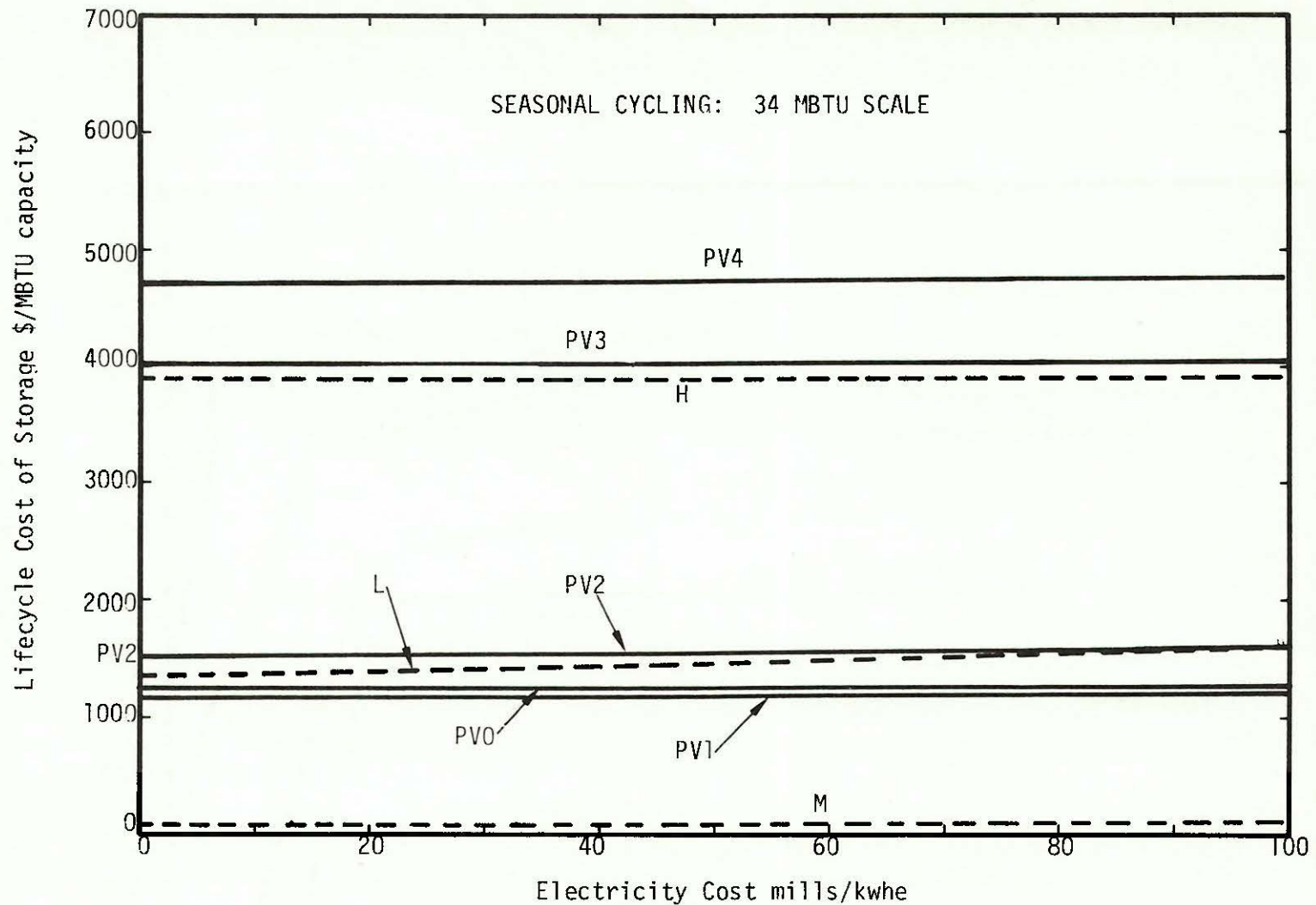


Figure 3. Seasonal cycling of storage for small quantities of hydrogen (34MBTU). Life cycle costs for seasonal storage are dominated by vessel costs, hence the flatness of the curves versus parasitic electricity costs. See Table II for key to curve designators.

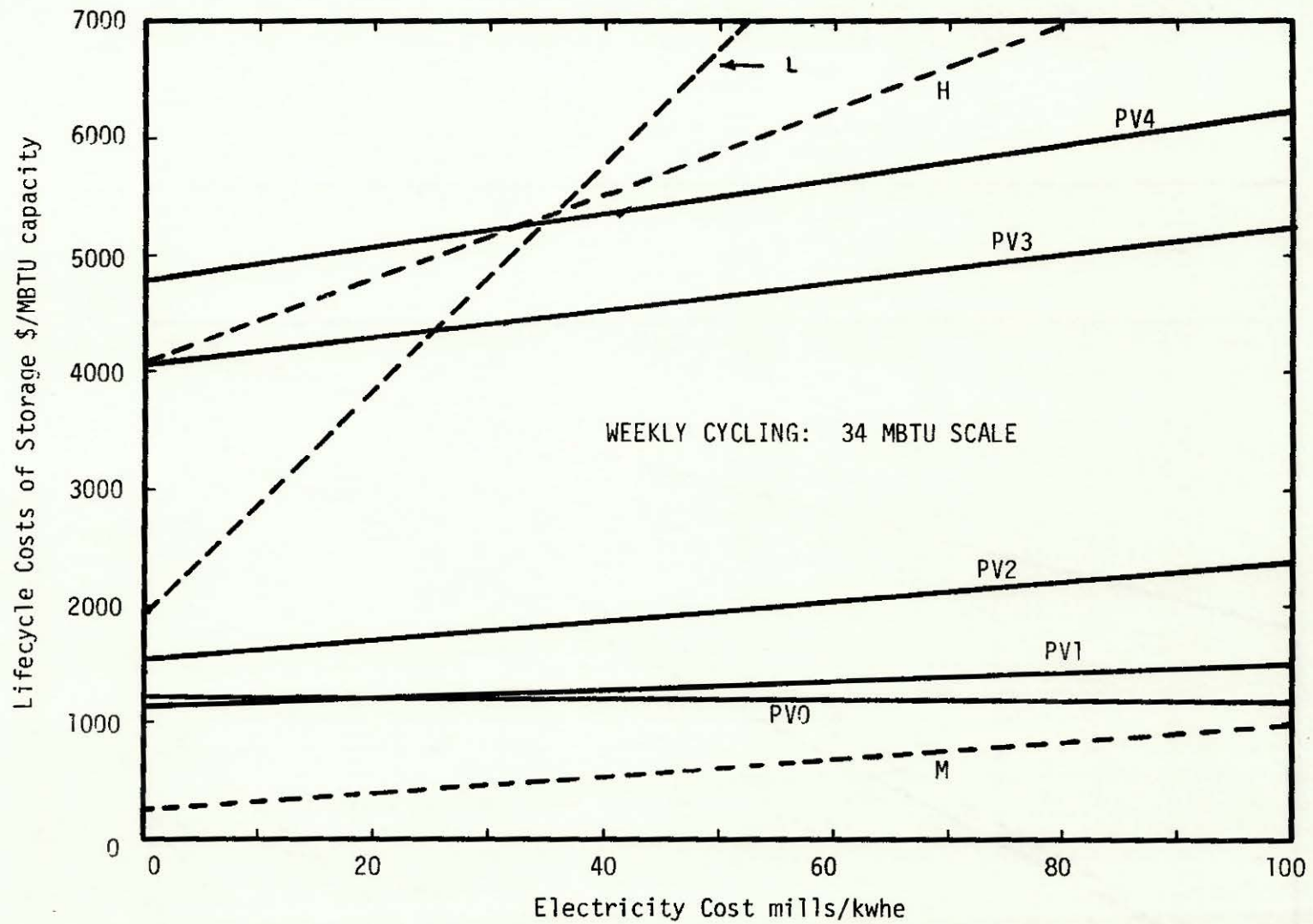


Figure 4. Weekly cycling of storage for small quantities of hydrogen (34MBTU). Weekly storage is 52 times as energy intensive as seasonal, hence the curves are steeper. See the key to curve designators in Table II.

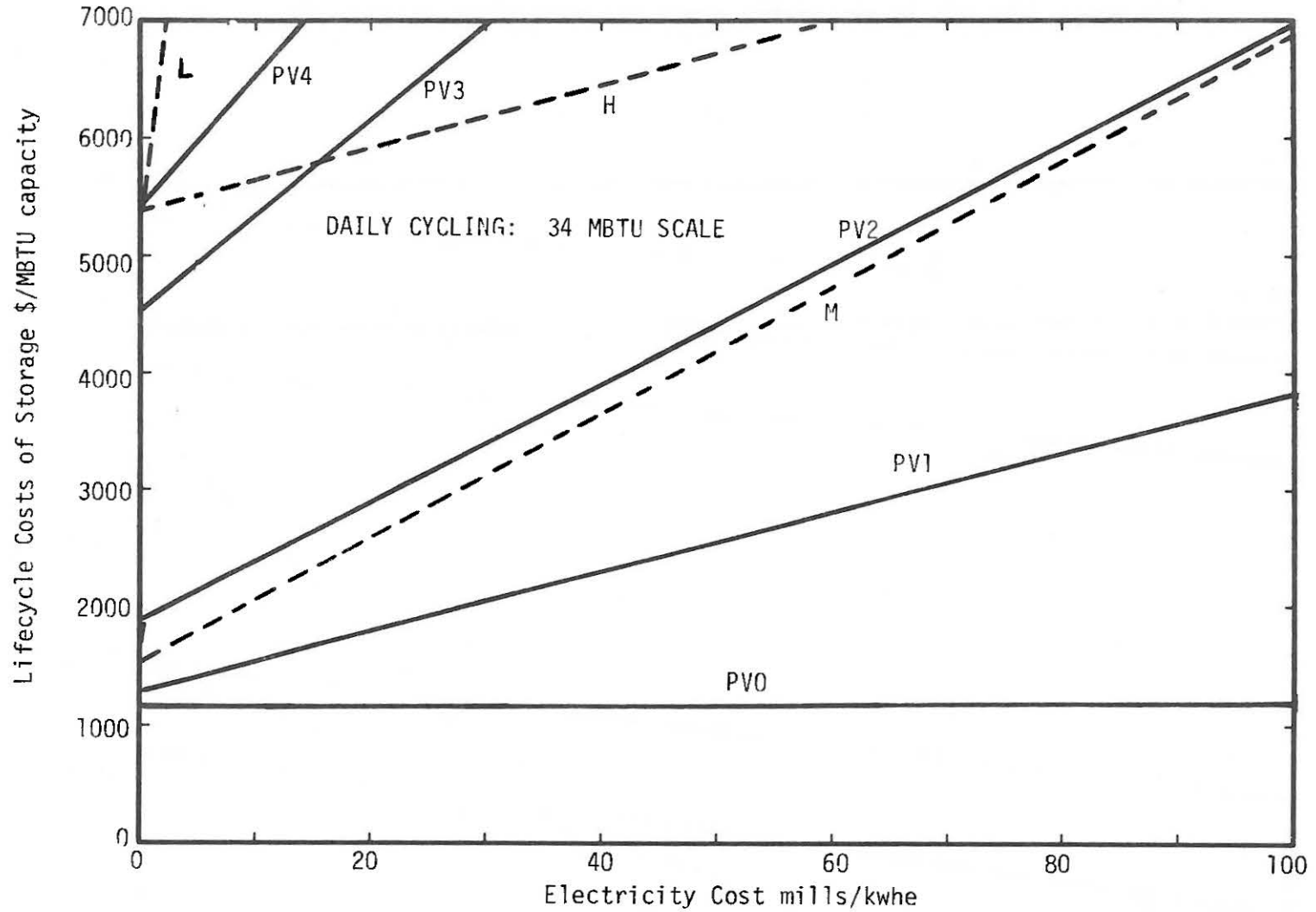


Figure 5. Daily cycling of storage for small quantities of hydrogen (34MBTU). Daily cycling is very energy intensive, hence the least expensive system is PV0 which requires no compression. See Table II for key to designators.

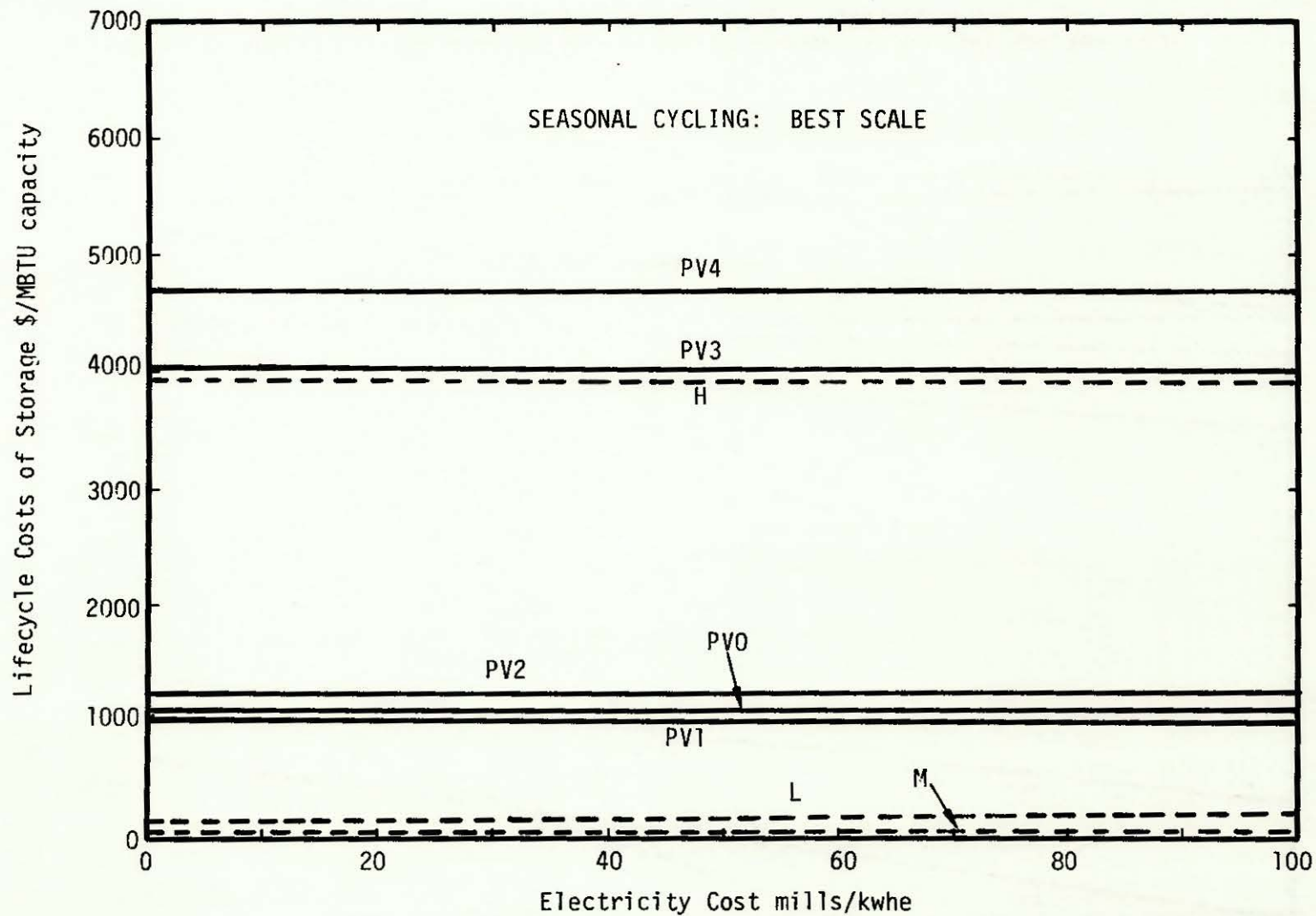


Figure 6. Seasonal cycling of storage for the best quantity of hydrogen for each technology. See Table II for key to curve designators.

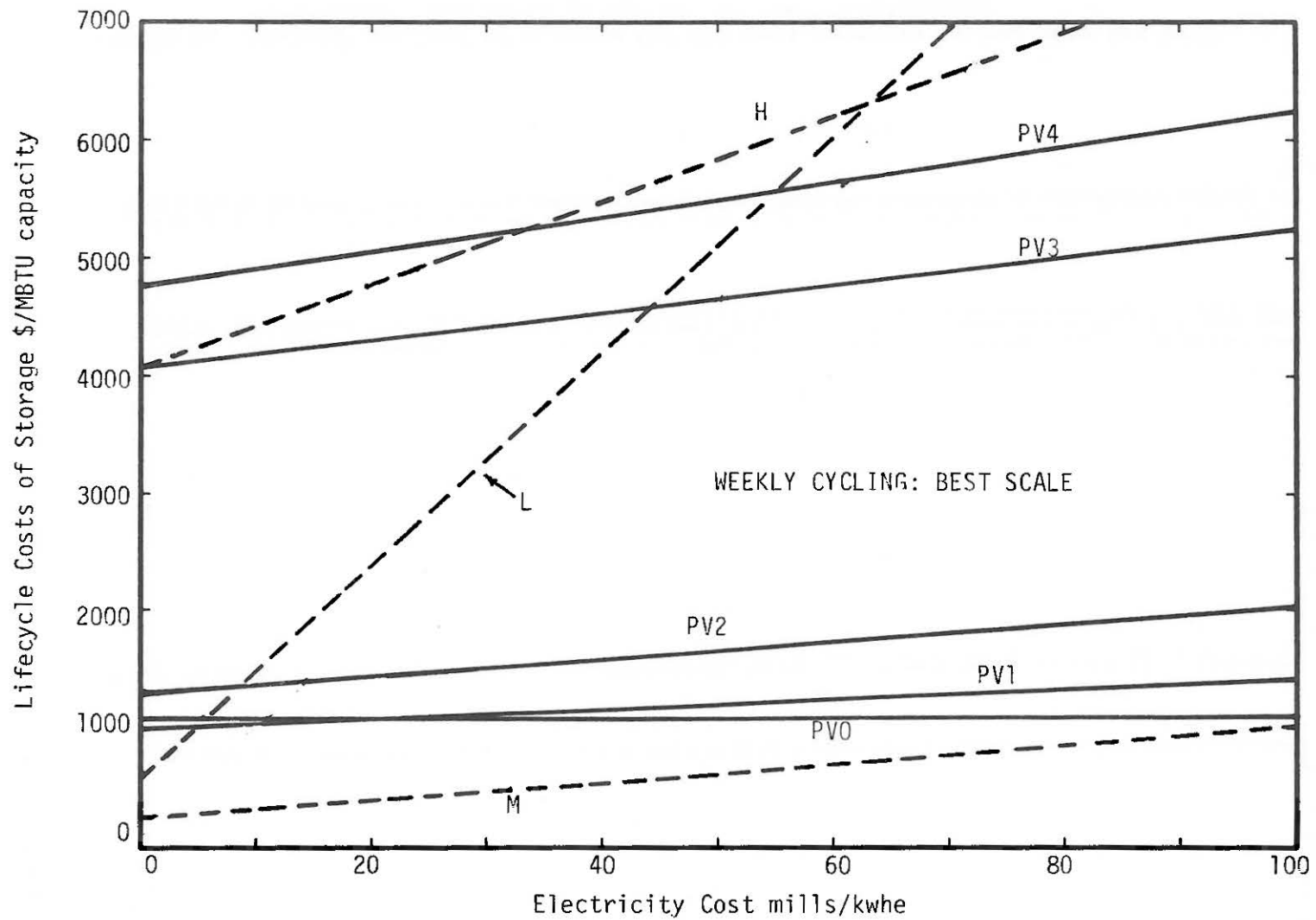


Figure 7. Weekly cycling of storage for the best quantity of hydrogen for each technology. See Table II for key to curve designators.

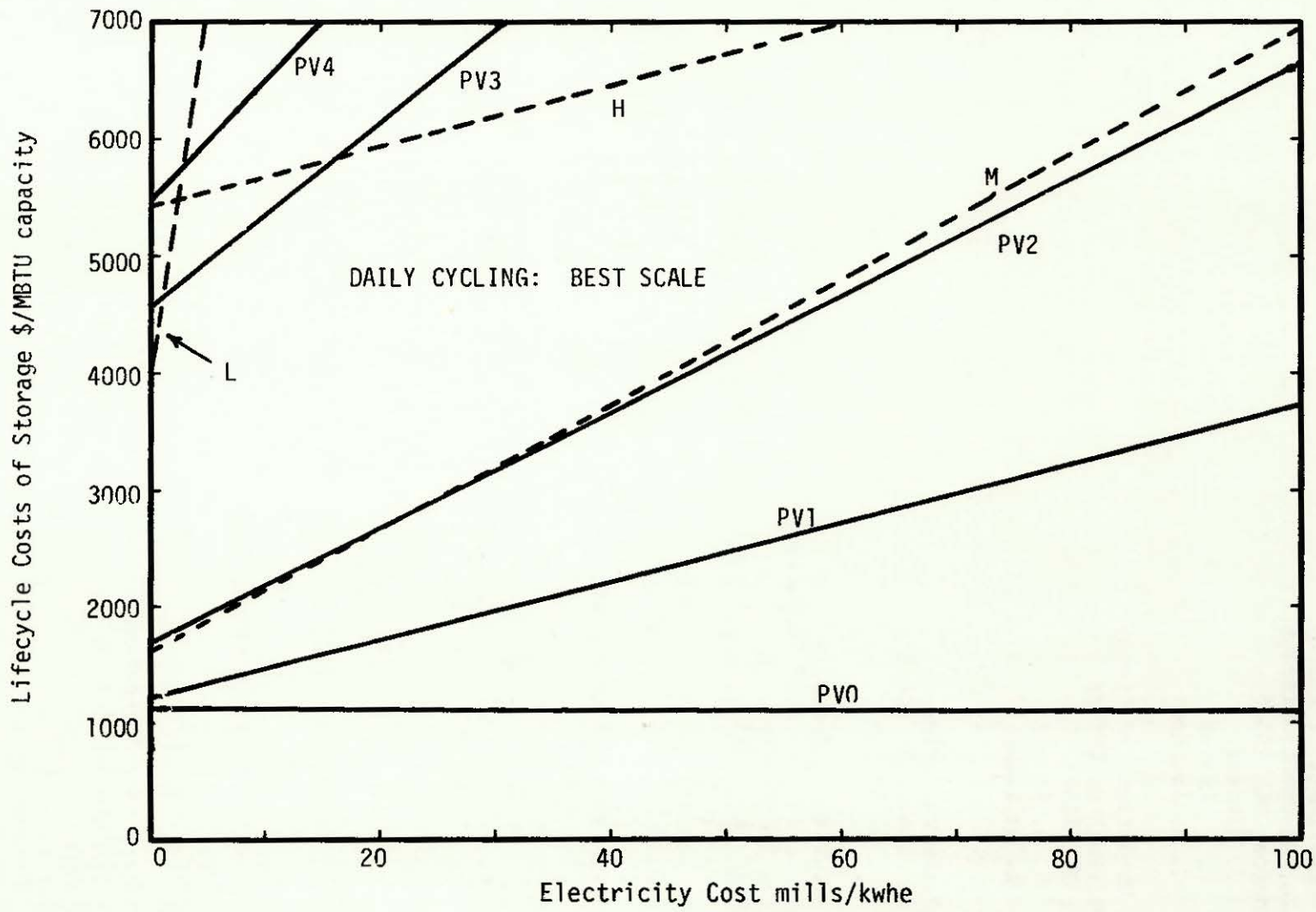


Figure 8. Daily cycling of storage for the best quantity of hydrogen for each technology. See key to curve designators in Table II.

DISTRIBUTION:

U. S. Department of Energy  
Division of Energy Storage  
Washington, DC 20545  
ATTN: J. Gahimer  
R. R. Reeves  
J. H. Swisher

U. S. Department of Energy  
Brookhaven Area Office  
Upton, NY 11973  
ATTN: R. A. Friess  
L. Williams

NASA  
Ames Research Center  
Mountain View, CA 94040  
ATTN: H. G. Nelson

Jet Propulsion Laboratory  
California Institute of Technology  
4800 Oak Grove Drive  
Pasadena, CA 91103  
ATTN: R. Hagler  
R. H. Turner  
J. H. Kelly

Brookhaven National Laboratory  
Upton, NY 11973  
ATTN: A. Mezzina, Bld. 120  
M. Rosso, Bld. 835  
F. J. Salzano, Bld. 120  
G. Strickland, Bld. 120

J. Harris  
Pratt and Whitney Aircraft Group  
P.O. Box 269  
West Palm Beach, FL 33402

Dr. M. R. Louthan, Jr.  
Virginia Polytechnic Institute and  
State University  
Blacksburg, VA 24061

Institute of Gas Technology  
3424 South State Street  
IGT Center  
Chicago, IL 60616  
ATTN: D. Gregory  
J. Pangborn

R. E. Eiber  
Battelle Memorial Institute  
Pacific Northwest Laboratory  
P.O. Box 999  
Richland, WA 99352

R. Teitel  
Robert J. Teitel Associates  
P.O. Box 81921  
San Diego, CA 92138

R. D. Smith  
Rocket Research Company  
York Center  
Redmond, WA 98052

Solar Energy Research Institute  
1536 Cole Boulevard  
Golden, CO 80401  
ATTN: R. Copeland  
C. Wyman

P. O. Carden  
Energy Conversion Group  
Department of Engineering Physics  
Australian National University  
Canberra, ACT 2600  
AUSTRALIA

Mr. T. S. Gold  
c/o OATSD (AE)  
Rm. 3E1069, Pentagon  
Washington, DC 20301

H. M. Stoller, 4730  
F. L. Vook, 5100; Attn: G. A. Samara, 5130  
J. E. Schirber, 5150  
R. S. Claassen, 5800; Attn: M. J. Davis, 5830  
T. B. Cook, 8000  
W. J. Spencer, 8100  
A. N. Blackwell, 8200  
B. F. Murphey, 8300  
D. M. Schuster, 8310  
W. R. Hoover, 8312 (10)  
R. W. Mar, 8313  
S. L. Robinson, 8314 (10)  
R. E. Stoltz, 8314 (10)  
A. J. West, 8314  
L. A. West, 8315  
J. R. Spingarn, 8316 (10)  
J. C. Swearingen, 8316  
R. L. Rinne, 8320

J. J. Iannucci, 8326 (10)

L. D. Hostetler, 8328

S. C. Keeton, 8352

W. Bauer, 8340

W. D. Wilson, 8341

L. Gutierrez, 8400

R. C. Wayne, 8450

P. J. Eicker, 8451

J. D. Fish, 8452

A. C. Skinrod, 8452

T. T. Bramlette, 8453

W. G. Wilson, 8453

Publications Division, 8265, for TIC (27)

Publications Division, 8265/Technical Library Processes and Systems Division, 3141

Technical Library Processes and Systems Division, 3141 (2)

Library and Security Classification Division, 8266 (3)

